Chemical Geology 412 (2015) 151–166

Contents lists available at ScienceDirect

Chemical Geology

journal homepage: www.elsevier.com/locate/chemgeo

# Applications and limitations of U–Th disequilibria systematics for determining ages of carbonate alteration minerals in peridotite

Evelyn M. Mervine [a,*,1], Kenneth W.W. Sims [b], Susan E. Humphris [c], Peter B. Kelemen [d]

[a] MIT/WHOI Joint Program, Geology and Geophysics Department, Woods Hole Oceanographic Institution, 266 Woods Hole Road, Woods Hole, MA 02543, USA
[b] Geology and Geophysics Department, University of Wyoming, 1000 East University Avenue, Laramie, WY 82071, USA
[c] Geology and Geophysics Department, Woods Hole Oceanographic Institution, 266 Woods Hole Road, Woods Hole, MA 02543, USA
[d] Lamont-Doherty Earth Observatory, 61 Route 9W, Palisades, NY 10964, USA

ARTICLE INFO

*Article history:*
Received 13 February 2015
Received in revised form 19 July 2015
Accepted 20 July 2015
Available online 22 July 2015

*Keywords:*
Carbonate
Peridotite
Uranium
Thorium
U-series dating
Ophiolite

ABSTRACT

$^{238}U$–$^{234}U$–$^{230}Th$ dating was conducted on carbonate alteration minerals in the peridotite layer of the Samail Ophiolite, Sultanate of Oman, in order to assess the applicability of U-series dating techniques to these types of Quaternary terrestrial carbonates and also to further constrain natural rates of carbonation of the peridotite. Due to their low U concentrations and relatively high Th/U ratios, Samail carbonates are challenging to date with the $^{230}Th$ technique because of the sensitivity of ages to corrections for initial $^{230}Th$. Uncorrected $^{230}Th$ ages for Ca-rich travertines are consistently older than previously obtained $^{14}C$ ages. However, geologically reasonable initial $^{230}Th$ corrections bring the two sets of ages into concordance. This age concordance suggests that the travertines are generally closed systems, adding a level of credence to the reliability of previously obtained $^{14}C$ ages. In contrast, uncorrected $^{230}Th$ ages for Mg-rich carbonate veins are generally younger than previously obtained $^{14}C$ ages. These young ages are interpreted in terms of remobilization of hexavalent U, which is subsequently deposited as tetravalent U by reduced serpentinization fluids. Two Mg-rich carbonate veins sampled at a roadcut have near-equilibrium ($^{230}Th/^{238}U$) and ($^{234}U/^{238}U$) values, which indicate that these veins are >375,000 years in age, consistent with their "$^{14}C$ dead" (>50,000 years BP) ages. The variable young and old ages for these Mg-rich carbonate veins indicate that carbonation of the peridotite layer of the Samail Ophiolite is an ongoing process and that there have been multiple generations of subsurface carbonate vein formation. Overall, this study provides insights into some of the challenges associated with applying U-series dating methods to Quaternary terrestrial carbonates, in particular carbonate alteration minerals in peridotites, and highlights some areas where there is room for improvement, such as obtaining better constraints on the isotopic composition of admixed detritus, and also some advantages, such as the ability to identify open system behavior not apparent from $^{14}C$ dating and stable C and O isotopic analysis alone.



## 1. Introduction

Determining timescales of the formation and preservation of carbonate alteration minerals in mantle peridotite is essential in order to better understand the role of this potentially important sink in the global carbon cycle and also to evaluate the feasibility of using artificially enhanced, *in situ* formation of carbonates in peridotite as a method for mitigating the buildup of anthropogenic $CO_2$ emissions in the atmosphere (e.g. Seifritz, 1990; Lackner et al., 1995; Lackner, 2002; Kelemen and Matter, 2008; Matter and Kelemen, 2009; Kelemen et al., 2011). While natural carbonation of peridotite is commonly observed subaerially and on the seafloor (e.g. Trommsdorff and Evans, 1977; Trommsdorff et al., 1980; Ferry, 1995; Surour and Arafa, 1997; Kelley et al., 2001, 2005; Früh-Green et al., 2003; Ludwig et al., 2006, 2011; Kelemen and Matter, 2008; Matter and Kelemen, 2009; Power et al., 2009; Kelemen et al., 2011; Pronost et al., 2011; Beinlich and Austrheim, 2012; Harrison et al., 2013; Chavagnac et al., 2013a, 2013b; Mervine et al., 2014), the natural rate of peridotite carbonation and therefore the rate of $CO_2$ uptake via this alteration mechanism is poorly known (e.g. Wilson et al., 2006, 2009a, 2009b; Kelemen and Matter, 2008; Kelemen et al., 2011; Mervine et al., 2014). In part, this is because carbonate alteration minerals in peridotite are challenging to date. Several studies (e.g. Kelemen and Matter, 2008; Wilson et al., 2009b; Kelemen et al., 2011; Mervine et al., 2014) have employed $^{14}C$ dating, but this dating technique has a practical limit of only ~50,000 years. Use of the $^{238}U$–$^{234}U$ and $^{234}U$–$^{230}Th$ disequilibria dating techniques (which have practical dating

* Corresponding author.
*E-mail addresses:* emervine@whoi.edu, Evelyn.Mervine@debeersgroup.com (E.M. Mervine), ksims7@uwyo.edu (K.W.W. Sims), shumphris@whoi.edu (S.E. Humphris), peterk@ldeo.columbia.edu (P.B. Kelemen).
[1] Present address: De Beers Marine, DBM Gardens, Golf Park 2, Raapenberg Road, Pinelands, 7405, Cape Town, South Africa.

http://dx.doi.org/10.1016/j.chemgeo.2015.07.023
0009-2541/

limits of ~1 million years and ~375,000 years, respectively) and the U–Pb dating technique (which is suitable for dating on timescales of millions of years) to investigate longer timescales of carbonation is limited by the generally low (ppb level) U concentrations of peridotites and their associated carbonate alteration minerals (e.g. Hanhøj et al., 2010; Bodinier and Godard, 2014). Carbonates formed in peridotites at the Lost City Hydrothermal Field, which is located off-axis of the Mid-Atlantic Ridge, have been dated using U–Th disequilibria techniques (Ludwig et al., 2011). However, these carbonates have high U concentrations (ppm level) due to contribution of U from seawater (Ludwig et al., 2011). Historically, little work has been done to apply the U–Pb dating technique to carbonates although recently there has been some development in this field, with a focus on dating of speleothem samples with high U and low common Pb concentrations (e.g. Rasbury and Cole, 2009; Woodhead and Pickering, 2012; Hellstrom and Pickering, 2015).

Furthermore, while some carbonates, particularly corals and speleothems, are routinely dated with U–Th disequilibria methods (e.g. Edwards et al., 2003), dating of terrestrial carbonates with these techniques can be challenging due to the significant presence of admixed detritus. Unlike most corals and speleothems, terrestrial carbonates are usually affected by the presence of initial $^{230}$Th and, to a lesser extent, by $^{234}$U and $^{238}$U contributed by detrital material (e.g. Bischoff and Fitzpatrick, 1991; Luo and Ku, 1991; Kaufman, 1993). This detritus is often fine-grained and intergrown with the carbonate, making physical separation very difficult (e.g. Ku and Liang, 1984; Bischoff and Fitzpatrick, 1991; Luo and Ku, 1991). Various approaches have been attempted over the years to account for detrital $^{230}$Th, $^{234}$U, and $^{238}$U in terrestrial carbonates, including light acid leaching, separating the carbonate material from the admixed detritus, and pseudoisochron methods for determining the composition of incorporated detritus (e.g. Osmond et al., 1970; Schwarcz and Lathan, 1989; Przybylowicz et al., 1991; Bischoff and Fitzpatrick, 1991; Luo and Ku, 1991). However, these techniques have had limited success. In most cases, employing total sample dissolutions with corrections for detrital inputs is the most robust way to obtain U–Th disequilibria ages for terrestrial carbonates (e.g. Kaufman, 1993; Ludwig and Titterington, 1994; Edwards et al., 2003). However, terrestrial carbonates with low U concentrations and high Th/U ratios, such as carbonate alteration products formed in peridotites, can be challenging to date with U–Th disequilibria methods since the ages are highly sensitive to detrital corrections.

In this study we examined the applications and limitations of using U–Th disequilibria methods to date carbonate alteration minerals that formed in peridotites of the Samail Ophiolite, Sultanate of Oman (Fig. 1). The Samail Ophiolite is one of the largest and best-exposed ophiolites in the world (Glennie et al., 1973, 1974; Coleman, 1977, 1981; Lippard et al., 1986; Nicolas et al., 2000) and is thus an excellent location for investigating natural rates of carbonate formation in peridotite. The goal of this study was to determine $^{238}$U–$^{234}$U and $^{234}$U–$^{230}$Th ages and age limits for Samail carbonates in order to further assess the range of ages of carbonate alteration minerals in the peridotite layer of the Samail Ophiolite. This study builds upon previous $^{14}$C dating and stable C and O isotope analyses of Samail carbonates, which are presented in Mervine et al. (2014) and also in Clark and Fontes (1990), Clark et al. (1992), Kelemen and Matter (2008), and Kelemen et al. (2011). Because these Quaternary terrestrial carbonates contain significant admixed fine-grained detritus, we undertook methods to: (1.) attempt to separate the aluminosilicate detritus from the carbonate or (2.) accurately correct for the effect the detritus is having on the $^{238}$U–$^{234}$U–$^{230}$Th isotope systematics of the carbonate minerals. Comparing the $^{238}$U–$^{234}$U and $^{234}$U–$^{230}$Th ages and age limits determined for the Samail carbonates with previously published $^{14}$C ages on the same samples (Mervine et al., 2014) enabled us to carefully scrutinize the reliability of ages obtained with both dating systems and to further constrain timescales of natural carbonation of Samail Ophiolite peridotites.

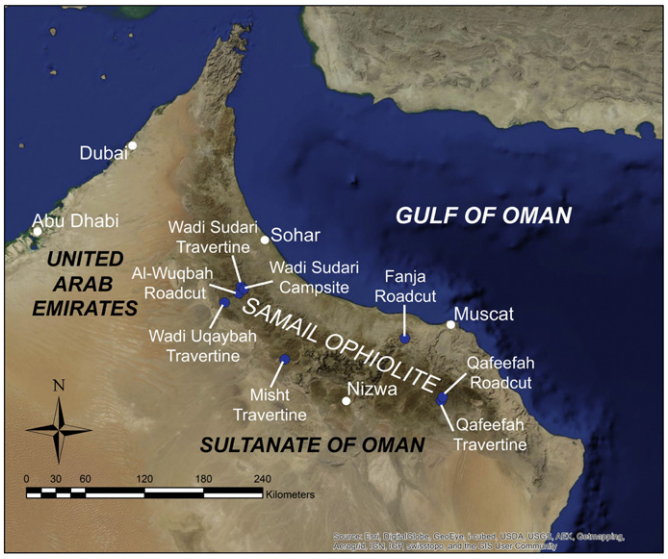


**Fig. 1.** The eight field locations (blue circles) where carbonate and peridotite samples were collected in the Samail Ophiolite during 2009 and 2010 field seasons. Map made using ArcGIS, Version 10.1.

## 2. Background

### 2.1. Terrestrial carbonates in the Samail Ophiolite

The Samail Ophiolite ranges from approximately 50 to 100 km in width and extends for greater than 500 km (e.g. Lippard et al., 1986; Nicolas et al., 2000). The ophiolite consists of several uplifted, thrust-bounded blocks (nappes) of oceanic crust and mantle that were obducted at ~80 to 95 Ma on top of autochthonous shelf carbonate rocks (the Hajar Supergroup) and parautochthonous continental slope carbonate rocks (the Sumeini Group), which rest on top of pre-Permian crystalline basement (Coleman, 1981; Lippard et al., 1986; Searle and Cox, 1999, 2002). These nappes consist of ~4 to 7 km of crustal rocks (layered gabbros, sheeted dikes, and volcanics, including pillow lavas) and ~8 to 12 km of upper mantle, primarily harzburgite (Glennie et al., 1973, 1974; Coleman, 1981; Lippard et al., 1986; Nicolas et al., 2000). Abundant carbonate veins as well as calcite-rich travertines are found throughout the peridotite layer of the ophiolite (e.g. Neal and Stanger, 1984, 1985; Clark and Fontes, 1990; Clark et al., 1992; Kelemen and Matter, 2008; Kelemen et al., 2011; Chavagnac et al., 2013a, 2013b; Mervine et al., 2014).

This study focuses on two types of carbonate alteration products that form in the peridotite layer of the Samail Ophiolite: (1.) travertine precipitated from high pH springs (Clark and Fontes, 1990; Clark et al., 1992; Kelemen and Matter, 2008; Kelemen et al., 2011; Paukert et al., 2012; Chavagnac et al., 2013a, 2013b; Mervine et al., 2014) and (2.) carbonate veins that form *in situ* in partially hydrated (serpentinized) peridotite (Matter and Kelemen, 2009; Kelemen et al., 2011; Streit et al., 2012; Mervine et al., 2014). These carbonates are thought to form as a result of low temperature alteration of peridotite through interaction with meteoric water (Fig. 2) (e.g. Barnes et al., 1967, 1978; Barnes and O'Neil, 1969, 1971; Neal and Stanger, 1985; Bruni et al., 2002; Cipolli et al., 2004; Kelemen et al., 2011). When meteoric water weathers partially serpentinized peridotite, $Mg^{2+}$–$HCO_3^-$ rich waters (known as "Type I" waters) are formed. As these waters percolate deeper into peridotite bedrock where they are no longer in equilibrium with the atmosphere, they precipitate Mg-rich carbonates, serpentines, and clays. As a result of this precipitation and other reactions in the subsurface, the waters transform into $Ca^{2+}$–$OH^-$ waters (known as "Type II" waters) that have very high pH (10 to 12) and low Mg, C, and oxygen fugacity (Eh approximately −200 mV) (Neal and Stanger, 1983, 1984, 1985; Clark and

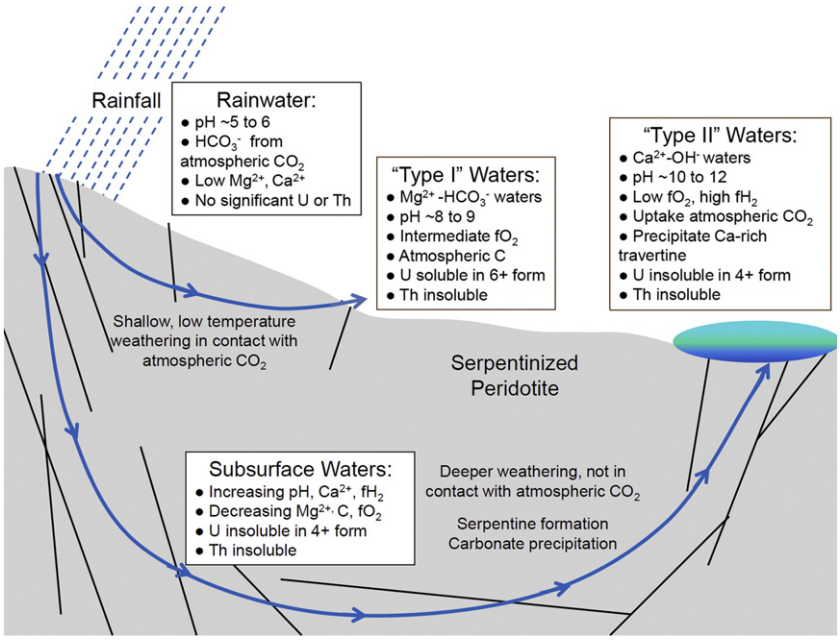


**Fig. 2.** Schematic illustrating the behavior of $CO_2$, U, and Th in Type I and Type II waters associated with alteration of fractured, partially-serpentinized peridotite. Figure modified from Neal and Stanger (1985).

Fontes, 1990; Kelemen and Matter, 2008; Kelemen et al., 2011; Paukert et al., 2012; Chavagnac et al., 2013a, 2013b). When Type II waters return to the surface as hyperalkaline springs, they rapidly react with atmospheric $CO_2$ to precipitate calcite-rich travertines (e.g. Clark and Fontes, 1990; Clark et al., 1992; Kelemen and Matter, 2008; Paukert et al., 2012; Chavagnac et al., 2013a, 2013b; Mervine et al., 2014).

The calcite-rich travertines (Fig. 3, Panels A to C) are precipitated from the hyperalkaline springs found throughout the Samail Ophiolite, predominantly in the peridotite layer and concentrated along the basal thrust of the ophiolite as well as along the crust-mantle boundary (Neal and Stanger, 1984, 1985; Clark and Fontes, 1990; Clark et al., 1992; Dewandel et al., 2003, 2004, 2005; Kelemen and Matter, 2008; Kelemen et al., 2011; Paukert et al., 2012; Chavagnac et al., 2013a, 2013b). At these springs, thick travertine deposits (up to several meters, on average ~1 to 2 m) form on top of peridotite, which is highly fractured with abundant carbonate-serpentine veins. Turquoise-blue alkaline pools lined with white carbonate precipitate are a feature of many hyperalkaline springs. Browner, more weathered (and generally older) travertine deposits are often found upslope and to the side of the actively precipitating travertine deposits (Kelemen and Matter, 2008; Mervine et al., 2014).

The carbonate veins (Fig. 3, Panels D to H) form *in situ* in the peridotite and, to a lesser extent, in the gabbro and basalt layers of the ophiolite (Kelemen and Matter, 2008; Kelemen et al., 2011; Mervine et al., 2014). Carbonate veins adjacent to surface travertine deposits are Ca-rich and similar in composition to the travertines. Carbonate veins sampled far from travertines are generally Mg-rich and presumably formed in the deeper subsurface during the transformation of Type I waters to Type II waters. The Mg-rich carbonate veins are predominately composed of magnesite and dolomite, range in size from a few millimeters to several meters thick, and can extend for hundreds of meters (Kelemen and Matter, 2008; Kelemen et al., 2011; Mervine et al., 2014). The Mg-rich carbonate veins are often intergrown with serpentine veins.

### 2.2. Previous dating of carbonate alteration minerals in peridotite in the Samail Ophiolite

Carbonate alteration minerals formed in the peridotite layer of the Samail Ophiolite have been previously dated by $^{14}C$, with ages reported in Clark and Fontes (1990), Clark et al. (1992), Kelemen and Matter (2008), Kelemen et al. (2011), and Mervine et al. (2014). Clark and Fontes (1990) and Clark et al. (1992) dated ~50 travertines and travertine veins sampled in the vicinity of four hyperalkaline springs near the town of Nizwa. They found that these travertines and travertine veins varied in age from >modern (post-1950) to ~35,000 years BP, with one sample "$^{14}C$ dead" (older than the ~50,000 year limit of $^{14}C$ dating). Kelemen and Matter (2008) and Kelemen et al. (2011) dated ~60 carbonates, both travertines and Mg-rich carbonate veins, from numerous locations throughout the southern ~2/3 of the ophiolite. Similar to the previous studies in the Nizwa area, they found that the travertines varied in age from > modern to ~40,000 years BP. They also found that the Mg-rich carbonate veins had an average $^{14}C$ age of ~26,000 years BP, an important observation since previously many of these veins were believed to be tens of millions of years old. Only two of their samples were $^{14}C$ dead. Mervine et al. (2014) obtained $^{14}C$ ages for an additional ~100 Samail carbonates, including several layered travertine terrace sequences. Evaluating all available $^{14}C$ data, Mervine et al. (2014) concluded that the travertines range in age from > modern to >45,000 years BP in age and that between ~30,000 and ~45,000 years BP the travertine deposition rate was ~0.1 to 0.3 mm/year for the four travertine sequences analyzed. Furthermore, they found that new travertine $^{14}C$ ages filled in previously observed "gaps" in the Clark and Fontes (1990) dataset, implying that travertine deposition has been fairly continuous and not necessarily controlled by climatic variations, as was previously hypothesized by Clark and Fontes (1990). Notably, Mervine et al. (2014) observed that a significant proportion of Mg-rich carbonate veins sampled at three roadcuts were $^{14}C$ dead. A location-weighted average indicates that ~40% of Mg-rich carbonate veins sampled at roadcuts are $^{14}C$ dead. In contrast, no Mg-rich carbonate veins sampled at outcrops (i.e. on the natural weathering surface of the peridotite) are $^{14}C$ dead. Mervine et al. (2014) concluded that there have been multiple generations of Mg-rich carbonate vein formation and that this vein formation continues to the present day. Furthermore, they speculated that some of the apparent $^{14}C$ ages for Mg-rich carbonate veins could be affected by open system behavior, such as dissolution and re-precipitation. Overall, the $^{14}C$ data indicate that carbonation of the peridotite layer of the Samail Ophiolite is a recent and on-going process and not exclusively an ancient one.

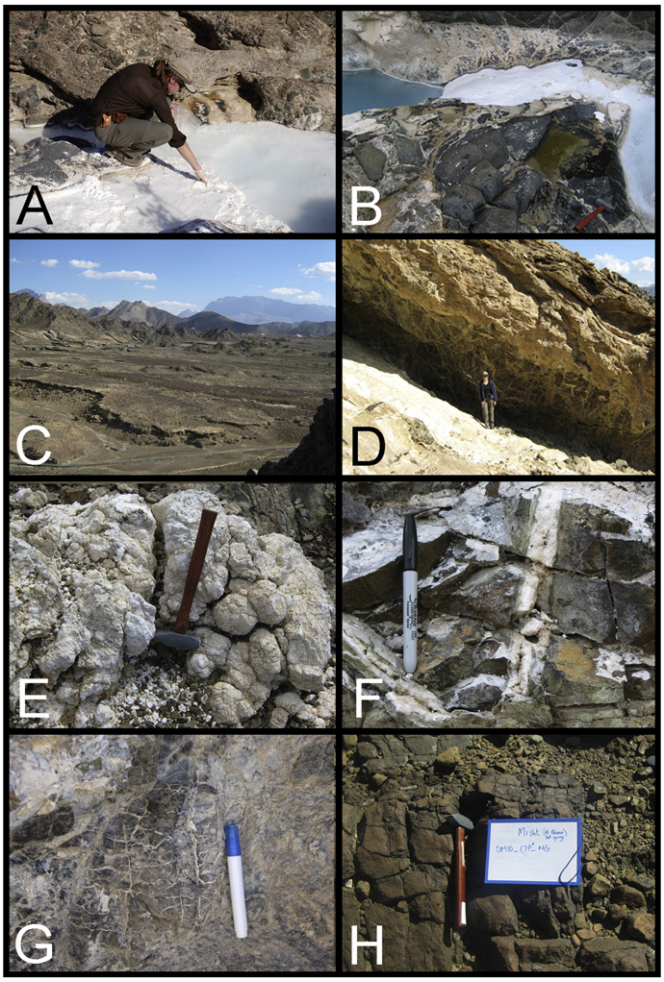


**Fig. 3.** Representative images of carbonates and altered peridotites in the Samail Ophiolite. A: Recently-formed travertine precipitate in a hyperalkaline streambed at Qafeefah Travertine. B: A turquoise hyperalkaline pool and recently-formed travertine precipitate at Wadi Sudari Travertine. Note the hammer for scale. C: Small hills of altered peridotite (background) adjacent to travertine terraces at Misht Travertine. D: Calcite-rich travertine veins exposed underneath a ~1 to 2 m thick travertine terrace deposit at Wadi Sudari Travetine. The veins can be seen in the overhang, next to the person. E: A white magnesite vein with botryoidal texture exposed on the natural peridotite weathering surface near Fanja Roadcut. Note the hammer for scale. F: Dolomite-serpentine veins exposed on the surface of Fanja Roadcut. Note the marker for scale. G: Very highly altered peridotite exposed underneath a travertine terrace at Misht Travertine. H: Highly altered peridotite exposed at Misht Travertine. Note the hammer for scale.

## 3. Methods

### 3.1. Sample descriptions

Sample descriptions are given in Table 1. Carbonates were collected from four locations (Fig. 1) of travertine deposition (Qafeefah Travertine, Misht Travertine, Wadi Uqaybah Travertine, and Wadi Sudari Travertine), from three roadcuts exposing carbonate veins in peridotite (Qafeefah Roadcut, Fanja Roadcut, and Al-Wuqbah Roadcut), and from one campsite located on the natural peridotite weathering surface and containing abundant carbonate veins exposed in outcrop (Wadi Sudari Campsite). All carbonates analyzed for U and Th were also dated with $^{14}C$ and analyzed for $\delta^{13}C$ and $\delta^{18}O$, the results of which have been previously reported in Mervine et al. (2014). Three water samples were collected from hyperalkaline pools at Wadi Sudari Travertine, Misht Travertine, and Wadi Dima (near Qafeefah, see Fig. 1) during January 2009 by Jürg Matter (University of Southampton). The water samples (500 mL) were filtered and acidified with ultrapure $HNO_3$ and were later analyzed for U and Th concentrations.

Three types of surficial travertines were analyzed for U and Th: (1.) recently-formed travertine precipitates collected from the bottoms of hyperalkaline pools (two samples), (2.) travertine terraces (four samples), and (3.) travertine "pseudospeleothems" (two samples), which are speleothem-like formations that have developed in overhangs, such as underneath travertine terraces. Note that these features are not true speleothems because they were not formed within caves. Also note that travertine terrace sample OM09-109C-MS is part of a younger travertine terrace forming between weathered, older travertine terraces; these travertines were distinguished as "channel-filling travertines" in Mervine et al. (2014). In addition, U and Th measurements were obtained for one Ca-rich travertine vein.

Mg-rich carbonate veins (13 samples) were also analyzed for U and Th. For the purposes of this study, these veins have been divided into "outcrop veins" (sampled from the natural peridotite weathering surface) and "roadcut veins" (sampled at roadcuts). Both types of veins are interpreted to have formed in the deeper subsurface; however, the roadcut veins are generally less weathered than the outcrop veins, which are often partially eroded. U and Th concentration measurements were also obtained for two serpentine mineral fractions that were separated out of intergrown carbonate-serpentine veins sampled at roadcuts.

Finally, U and Th measurements were obtained for two sediment samples, which are a potential source of detritus in the carbonates. These sediment samples were collected from small wadis or valleys adjacent to the carbonates sampled at Fanja Roadcut and Wadi Uqaybah Travertine. There is no significant soil formation at any of the carbonate sampling locations, so these sediments consist of loose detritus that contains fragments of peridotite and carbonate as well as aeolian particles.

### 3.2. Geochemical analyses

Carbonates selected for U and Th analysis were crushed using a jaw crusher and then purified through magnetic separation and hand picking. Many of the carbonate veins consist of multiple minerals (e.g. magnesite, calcite, dolomite, serpentine, brucite). Whenever possible, monomineralic (or nearly so) separates were prepared, and their purity was evaluated by powder X-ray diffraction (XRD) analysis at Woods Hole Oceanographic Institution using a Philips Analytical PW1830 XRD machine. Mineral identification was conducted using the International Center for Diffraction Data Powder Diffraction File. While large fragments of peridotite and serpentine were easily removed through magnetic separation and hand picking, fine-grained aluminosilicate material incorporated into the travertines and, to a lesser extent, into the subsurface carbonate veins was impossible to remove through physical separation. Note that the two recently-formed travertine precipitates (OM09-8COPS-MS and OM09-10COPS-MS) were not purified (aside from removing large, obvious peridotite clasts) due to their fine-grained nature.

For travertines, approximately 1 to 2 g of material was required for analysis. For Mg-rich carbonate veins, approximately 20 to 30 g of material was required because of their extremely low U and Th concentrations. For select Mg-rich carbonate veins as well as the two serpentine mineral separates, 1 to 2 g of material was first analyzed for U and Th concentrations in order to identify samples that were most promising for isotopic analysis (i.e. had the highest U concentrations). For the sediments, 2 to 10 g of a bulk powder was analyzed for each sample.

Carbonates selected for $^{230}Th$ analyses were completely dissolved using $HNO_3$, HF, $HClO_4$, and $H_3BO_3$. To investigate the behavior of samples during dissolution and also the nature of the incorporated aluminosilicate detritus, separate weak $HNO_3$ leaches were carried out for select samples. The aluminosilicate residues left behind by these weak $HNO_3$ leaches were also dissolved and analyzed separately. A progressive dissolution experiment was carried out on one travertine sample (OM09-107C-MS). The dissolution experiments are discussed in detail in the

**Table 1**
Sample locations and descriptions.

| Sample name: | Location: | UTM-easting: | UTM-northing: | Description: | Major minerals (XRD): | Trace minerals (XRD): |
|---|---|---|---|---|---|---|
| *Travertines:* | | | | | | |
| OM09-76C-MS-A (top) | Wadi Sudari Travertine | 0443115 | 2650257 | Layered pseudospeleothem (drop) | Calcite | None |
| OM09-76C-MS-C (bottom) | Wadi Sudari Travertine | 0443115 | 2650257 | Layered pseudospeleothem (drop) | Calcite | Unidentified clay |
| OM09-8COPS-MS | Wadi Sudari Travertine | 0443118 | 2650078 | Recently-formed travertine precipitate | Calcite | Aragonite, hydromagnesite?, unidentified clay |
| OM09-84C-MS | Wadi Sudari Travertine | 0443082 | 2650304 | Travertine vein | Calcite, brucite | Hydromagnesite?, unidentified clay |
| OM09-106C-MS-A (top) | Wadi Uqaybah Travertine | 0426245 | 2633924 | Travertine terrace | Calcite | None |
| OM09-106C-MS-B (bottom) | Wadi Uqaybah Travertine | 0426245 | 2633924 | Travertine terrace | Calcite | Unidentified clay |
| OM09-107C-MS | Wadi Uqaybah Travertine | 0426309 | 2633950 | Travertine terrace | Calcite | Unidentified clay |
| OM09-109C-MS | Wadi Uqaybah Travertine | 0426208 | 2633925 | Travertine terrace | Calcite | None |
| OM09-10COPS-MS | Wadi Uqaybah Travertine | 0426183 | 2633965 | Recently-formed travertine precipitate | Calcite | Quartz, unidentified clay |
| *Mg-rich carbonate outcrop veins:* | | | | | | |
| OM09-47C-MS | Fanja Roadcut | 0609304 | 2597565 | Carbonate outcrop vein | Magnesite | Unidentified clay |
| OM10-13C-MG | Fanja Roadcut | 0609451 | 2597416 | Carbonate outcrop vein | Magnesite | Dolomite, calcite |
| OM10-53C-MG | Al-Wuqbah Roadcut | 0440574 | 2643360 | Carbonate outcrop vein | Magnesite | None |
| OM09-91C-MS | Wadi Sudari Campsite | 0446151 | 2647471 | Carbonate outcrop vein | Magnesite | Calcite |
| OM10-82C-MG | Wadi Sudari Campsite | 0445905 | 2647602 | Carbonate outcrop vein | Magnesite | Dolomite, calcite, unidentified clay |
| OM10-84C-MG | Wadi Sudari Campsite | 0445991 | 2647684 | Carbonate outcrop vein | Brucite, calcite | Magnesite, dolomite, unidentified clay |
| *Mg-rich carbonate roadcut veins:* | | | | | | |
| OM09-35C-MS | Qafeefah Roadcut | 0647852 | 2537682 | Carbonate/serpentine roadcut vein | Magnesite | Chrysotile, unidentified clay |
| OM09-36C-MS | Qafeefah Roadcut | 0647818 | 2537657 | Carbonate roadcut vein | Magnesite | Calcite, dolomite |
| OM09-55C-MS | Fanja Roadcut | 0609351 | 2597507 | Carbonate/serpentine roadcut vein | Dolomite | Aragonite?, unidentified clay |
| OM09-57C-MS | Fanja Roadcut | 0609356 | 2597501 | Carbonate/serpentine roadcut vein | Dolomite | Aragonite?, calcite, unidentified clay |
| OM09-58C-MS | Fanja Roadcut | 0609370 | 2597506 | Carbonate roadcut vein | Dolomite, periclase? | Aragonite?, unidentified clay |
| OM09-63C-MS | Fanja Roadcut | 0609470 | 2597481 | Carbonate roadcut vein | Magnesite | Unidentified clay |
| OM10-52C-MG | Al-Wuqbah Roadcut | 0440396 | 2643047 | Carbonate roadcut vein | Magnesite | Halite?, unidentified clay |
| *Serpentines:* | | | | | | |
| OM10-27C-MG-SERP | Qafeefah Roadcut | 0647791 | 2537644 | Carbonate/serpentine roadcut vein | Lizardite | None |
| OM10-54C-MG-SERP | Al-Wuqbah Roadcut | 0440832 | 2643931 | Carbonate/serpentine roadcut vein | Lizardite | None |
| *Sediments:* | | | | | | |
| OM09-8S-MS | Fanja Roadcut | 0609493 | 2597536 | Sediment collected from wadi floor | Lizardite | Quartz, dolomite, magnesite, calcite |
| OM09-12S-MS | Wadi Uqaybah Travertine | 0426173 | 2633970 | Sediment collected from wadi floor | Quartz, calcite | Chrysotile, dolomite, enstatite, aragonite? |
| *Carbonate standard:* | | | | | | |
| JCp-1 | Ryukyu Islands, Japan | | | *Porites* coral | – | – |

Supplementary Information. In brief, the dissolution experiments indicate that both elemental and isotopic fractionation of U and Th occurs during partial dissolution of Samail carbonates. This fractionation is most significant for the surface travertines, which incorporate higher amounts of aluminosilicate detritus than the subsurface carbonate veins. The observed fractionation as a result of partial dissolutions reinforces the need to employ a total dissolution approach for $^{230}$Th dating of terrestrial carbonates that contain significant admixed detritus (e.g. Bischoff and Fitzpatrick, 1991; Luo and Ku, 1991).

After dissolution, U and Th were purified using two columns (see details in Ball et al., 2008 and Sims et al., 2008a). The first was a nitric anion column that removes U and Th from the rock matrix. The second was a hydrochloric anion column that separates U from Th. For large samples, U and Th were first co-precipitated with Fe hydroxide. For the Fe hydroxide precipitation, 3.5 mg of an ultrapure Fe ICP standard manufactured by Ricca Chemical was added to each sample (see Edwards et al., 1986 for discussion of the Fe-hydroxide precipitation step).

U and Th concentrations were measured by isotope dilution ICP-MS using $^{229}$Th and $^{233}$U spikes. The isotope dilution measurements were carried out on a Thermo Scientific Element 2 mass spectrometer at Woods Hole Oceanographic Institution following procedures detailed in Sims et al. (2008a). U and Th isotopes were measured on chromatographically separated U and Th aliquots on separate days by MC-ICP-MS on a Thermo Scientific Finnigan Neptune mass spectrometer at Woods Hole Oceanographic Institution using techniques described in Ball et al. (2008) and Sims et al. (2008a,b). For the Th isotopic measurements, $^{230}$Th was measured on the center SEM using the RPQ high abundance sensitivity filter, and $^{232}$Th was measured on an up-mass Faraday. Th isotope mass bias and SEM–Faraday yield were corrected for by sample standard bracketing using a $^{230}$Th/$^{232}$Th atom ratio of $11.380 \pm 0.170 \times 10^{-6}$ for IRMM 35 (see Sims et al., 2008b

for details). For the U isotopic measurements, $^{234}U$ was measured on the center SEM, and $^{235}U$ and $^{238}U$ were measured on up-mass Faradays. U isotopes were corrected for mass bias using both an internal correction and assuming that the samples have $^{235}U/^{238}U = 0.0072527$ (Cheng et al., 2000) and an external correction using CRM U010 for a mass bias and SEM–Faraday yield using the Richter and Goldberg (2003) values $^{235}U/^{238}U = 0.0101382$ and $^{234}U/^{238}U = 5.4483 \times 10^{-5}$ (see Ball et al., 2008 for details). For a matrix matched quality assurance standard, the carbonate standard (JCp-1) was analyzed for U and Th concentrations and isotopes (Tables 2 and 3). In addition, a large compilation of U and Th concentration and isotopic ratio measurements for five synthetic Th standards (IRMM 35, IRMM 36, UCSC ThA, WUN, and OU ThU) and six rock standards (UCSC TML, Icelandic ATHO, USGS BCR2, USGS W2, USGS BHVO-2, and LV18) that were analyzed at the same general time as this Oman study can be found in Sims et al. (2008a), which represents a concerted international effort of six labs (WHOI; UCSC; LLNL; UI Urbana; GEOMOC, AU; Bristol, UK) to cross calibrate these U-series standards. The same instrumentation, methods, and $^{229}Th$ and $^{233}U$ spikes were used in both this study and in Sims et al. (2008a). Total procedural blanks, including the acid used for sample introduction, are typically less than <4 pg ($1 \times 10^{10}$ atoms) for $^{238}U$ and <3 pg ($7 \times 10^{9}$ atoms) for $^{232}Th$. Blank levels for $^{234}U$ and $^{230}Th$ are un-measureable but are approximately $10^{-4}$ of $^{238}U$ and $10^{-5}$ of $^{232}Th$, respectively.

**Table 2**
U and Th concentrations. U and Th concentrations were measured by isotope dilution using a Thermo Scientific Element 2 high resolution sector-field ICP-MS at WHOI. Mass fractionation was corrected by sample-standard bracketing with CRM112A, using a linear interpolation of $^{235}U/^{238}U$ measurements of the standard. Errors include uncertainties in spike calibrations, in run measurement error, and in standards against which instrument measurements were calibrated. Italic font indicates replicate analyses, and bold font indicates the average of replicate analyses.

| Sample name: | U (ppm): | 2σ (%): | Th (ppm): | 2σ (%): | Th/U: | 2σ (%): |
|---|---|---|---|---|---|---|
| *Travertines:* | | | | | | |
| OM09-76C-MS-A (top) | 0.0447 | 3.14 | 0.0673 | 1.45 | 1.5070 | 3.46 |
| OM09-76C-MS-C (bottom) | 0.0195 | 1.81 | 0.0472 | 1.83 | 2.4239 | 2.58 |
| OM09-8COPS-MS | 0.0596 | 1.95 | 0.1561 | 1.30 | 2.6202 | 2.35 |
| OM09-84C-MS | 0.0161 | 1.42 | 0.0041 | 1.39 | 0.2532 | 1.99 |
| OM09-106C-MS-A (top) | 0.8275 | 5.42 | 0.2917 | 1.96 | 0.3525 | 5.77 |
| OM09-106C-MS-B (bottom) | *0.3434* | *1.57* | *0.1507* | *2.20* | *0.4389* | *2.70* |
| | *0.3456* | *1.88* | *0.1507* | *1.25* | *0.4361* | *2.26* |
| | **0.3445** | **1.73** | **0.1507** | **1.73** | **0.4375** | **2.48** |
| OM09-107C-MS | 0.6016 | 1.52 | 0.4250 | 1.25 | 0.7065 | 1.96 |
| OM09-109C-MS | 0.0687 | 1.61 | 0.1072 | 1.98 | 1.5607 | 2.55 |
| OM09-10COPS-MS | *0.2693* | *3.06* | *0.3455* | *4.20* | *1.2829* | *5.19* |
| | *0.1732* | *1.56* | *0.3560* | *1.52* | *2.0551* | *2.18* |
| | **0.2213** | **2.31** | **0.3507** | **2.86** | **1.5852** | **1.24** |
| *Mg-rich carbonate outcrop veins:* | | | | | | |
| OM09-47C-MS | *0.0030* | *2.62* | *0.0007* | *2.10* | *0.2317* | *3.36* |
| | *0.0007* | *7.05* | *0.0003* | *3.44* | *0.3547* | *7.85* |
| | **0.0019** | **4.84** | **0.0005** | **2.77** | **0.2554** | **5.60** |
| OM10-13C-MG | 0.0010 | 1.65 | 0.0002 | 4.49 | 0.1683 | 4.78 |
| OM10-53C-MG | 0.0032 | 2.72 | 0.0006 | 2.48 | 0.1819 | 3.69 |
| OM09-91C-MS | 0.0114 | 8.72 | 0.0030 | 12.68 | 0.2626 | 15.39 |
| OM10-82C-MG | 0.0009 | 3.96 | 0.0003 | 2.45 | 0.2903 | 4.66 |
| OM10-84C-MG | 0.0010 | 1.74 | 0.0021 | 2.66 | 1.9955 | 3.18 |
| *Mg-rich carbonate roadcut veins:* | | | | | | |
| OM09-35C-MS | 0.0001 | 1.43 | 0.0003 | 1.31 | 3.0990 | 1.93 |
| OM09-36C-MS | 0.0001 | 2.11 | 0.0003 | 4.87 | 2.9332 | 5.30 |
| OM09-55C-MS | 0.0008 | 1.86 | 0.0004 | 2.55 | 0.4777 | 3.15 |
| OM09-57C-MS | 0.0053 | 1.46 | 0.0005 | 1.45 | 0.0978 | 2.06 |
| OM09-58C-MS | 0.0148 | 1.66 | 0.0002 | 2.65 | 0.0111 | 3.12 |
| OM09-63C-MS | *0.00003* | *4.47* | *0.00006* | *5.21* | *2.1948* | *6.86* |
| | *0.00004* | *2.72* | *0.00008* | *1.54* | *1.8916* | *3.13* |
| | **0.00003** | **3.59** | **0.00007** | **3.37** | **2.0121** | **4.99** |
| OM10-52C-MG | 0.0003 | 2.08 | 0.0017 | 6.37 | 5.6094 | 6.70 |
| *Serpentines:* | | | | | | |
| OM10-27C-MG-SERP | 0.00031 | 2.66 | 0.0003 | 2.06 | 1.0655 | 3.37 |
| OM10-54C-MG-SERP | 0.00045 | 2.11 | 0.0009 | 1.53 | 2.0371 | 2.61 |
| *Sediments:* | | | | | | |
| OM09-8S-MS | 0.1210 | 2.11 | 0.0686 | 2.35 | 0.5669 | 3.16 |
| OM09-12S-MS | 0.9055 | 3.91 | 1.3124 | 6.66 | 1.4494 | 7.72 |
| *Carbonate standard:* | | | | | | |
| JCp-1 | *2.7300* | *2.47* | *0.0502* | *3.36* | *0.0184* | *4.17* |
| | *2.7503* | *1.51* | *0.0505* | *2.29* | *0.0184* | *2.74* |
| | *2.7616* | *1.91* | *0.0510* | *2.17* | *0.0185* | *2.38* |
| | *2.8075* | *2.55* | *0.0572* | *2.83* | *0.0204* | *3.81* |
| | **2.7623** | **2.11** | **0.0522** | **2.66** | **0.0189** | **3.28** |

## 4. Results

### 4.1. Mineralogy

The results of X-ray diffraction analysis of powdered samples are presented in Table 1. Minerals were identified as “major” or “minor” but were not further quantified.

The mineralogy of the Samail carbonates is discussed in detail in Mervine et al. (2014). In brief, the travertine samples consist predominately of calcite with trace quantities of unidentified clay minerals. One recently-formed travertine precipitate (OM09-8COPS-MS) also contains minor aragonite and possibly hydromagnesite. The other recently-formed travertine precipitate (OM09-12S-MS) contains trace quartz, possibly from aeolian sand incorporated into the sample. The Mg-rich subsurface carbonate veins consist primarily of magnesite or dolomite except for one sample (OM10-84C-MG), which consists primarily of brucite.

The two sediment samples have distinct mineral compositions. The first sample collected near Fanja Roadcut (OM09-8S-MS) consists primarily of lizardite with minor quartz, dolomite, magnesite, and calcite. The second sample collected near Wadi Uqaybah Travertine (OM09-12S-MS) consists primarily of quartz and calcite with minor chrysotile, dolomite, enstatite, and possibly aragonite. The difference in mineralogy reflects the different detrital inputs from the nearby environment and also from aeolian sources at these two locations.

### 4.2. U and Th concentrations

Samail carbonates have U and Th concentrations ranging over several orders of magnitude from <1 ppb to ~1 ppm (Table 2 and Fig. 4). The travertine terraces and wadi sediments have the highest U and Th concentrations, ranging from ~0.1 to ~1 ppm for both U and Th. The Mg-rich carbonate veins have U and Th concentrations ranging from <1 ppb to ~10 ppb, three or four orders of magnitude lower than most of the travertine U and Th concentrations. Sample OM09-63C-MS, an Mg-rich carbonate vein, has U and Th concentrations comparable to the total procedural blank and thus below detection limit. The two serpentine mineral separates (from serpentine-carbonate veins) have very low (<1 ppb) U and Th concentrations comparable with those of the Mg-rich carbonate veins. The three hyperalkaline (500 mL) water samples analyzed by isotope dilution were well below the instrumental detection limits for U and Th, which are ~1 ppt. Reproducibility of U and Th concentration measurements for JCp-1 ($n = 4$) is better than the propagated analytical error of the individual measurements. The reproducibility of the travertine samples and Mg carbonate samples is also quite good with the exception of OM09-47C-MS, which is likely due to this sample's low U and Th concentrations and potential for heterogeneity from fine-grained admixed material.

### 4.3. U and Th isotopes

U and Th isotopic data are presented in Table 3. Note that in the tables, and throughout this paper, parentheses indicate activities. Due to low U and Th concentrations, only a subset of the samples analyzed for U and Th concentrations could be analyzed for U and Th isotopes.

**Table 3**
U and Th isotopic values. Isotopic compositions were measured with a Thermo Scientific Neptune MC-ICP-MS at WHOI. $^{232}$Th and $^{238}$U were measured on a Faraday cup, and $^{230}$Th was measured on an axial, discrete dynode ion counter with a repelling potential quadrupole (RPQ). Abundance sensitivity over 2 AMU at 85% transmission was ~50 ppb. An exponential correction was used to correct for the tailing of $^{232}$Th on $^{230}$Th. Use of UCSC Th 'A' for Th-bracketing results in inter-day reproducibility of 0.4–1.5% (2σ). $^{236}$U/$^{238}$U ratios of CRM U010 were measured to correct for mass bias drift and to calibrate SEM yield. Standard-sample-standard bracketing was used for U analyses. Italic font indicates replicate analyses, and bold font indicates the average of replicate analyses.

| Sample name: | $^{234}$U/$^{238}$U (×10$^{-6}$): | 2σ (%): | $^{230}$Th/$^{232}$Th (×10$^{-6}$): | 2σ (%): | ($^{234}$U/$^{238}$U): | 2σ (%): | ($^{230}$Th/$^{232}$Th): | 2σ (%): | ($^{238}$U/$^{232}$Th): | 2σ (%): | ($^{230}$Th/$^{238}$U): | 2σ (%): | Uncorrected $^{230}$Th age: |
|---|---|---|---|---|---|---|---|---|---|---|---|---|---|
| *Travertines:* | | | | | | | | | | | | | |
| OM09-76C-MS-A | 64.815 | 0.139 | 7.503 | 0.226 | 1.181 | 0.139 | 1.389 | 0.226 | 2.013 | 3.460 | 0.690 | 3.470 | 93,000 |
| OM09-76C-MS-C | 64.296 | 0.205 | 6.344 | 0.335 | 1.172 | 0.205 | 1.174 | 0.335 | 1.252 | 2.579 | 0.938 | 2.600 | 163,000 |
| OM09-8COPS-MS | 62.190 | 0.159 | 7.434 | 0.136 | 1.133 | 0.159 | 1.376 | 0.136 | 1.158 | 2.347 | 1.188 | 2.351 | – |
| OM09-84C-MS | 45.670 | 0.234 | 32.149 | 0.462 | 0.832 | 0.234 | 5.950 | 0.462 | 11.980 | 1.989 | 0.497 | 2.042 | 104,000 |
| OM09-106C-MS-A | 63.466 | 0.048 | 20.330 | 0.098 | 1.156 | 0.048 | 3.763 | 0.098 | 8.606 | 5.765 | 0.437 | 5.766 | 51,000 |
| OM09-106C-MS-B | *63.427* | *0.076* | *14.707* | *0.171* | *1.156* | *0.076* | *2.722* | *0.171* | *6.912* | *2.705* | *0.394* | *2.710* | |
| | *63.390* | *0.079* | *14.693* | *0.090* | *1.155* | *0.079* | *2.719* | *0.090* | *6.956* | *2.258* | *0.391* | *2.260* | |
| | **63.409** | **0.077** | **14.700** | **0.131** | **1.155** | **0.077** | **2.721** | **0.131** | **6.934** | **2.481** | **0.392** | **2.485** | **45,000** |
| OM09-107C-MS | 68.860 | 0.064 | 23.603 | 0.082 | 1.255 | 0.064 | 4.369 | 0.082 | 4.294 | 1.963 | 1.017 | 1.964 | 164,000 |
| OM09-109C-MS | 61.355 | 0.118 | 7.694 | 0.218 | 1.118 | 0.118 | 1.424 | 0.218 | 1.944 | 2.552 | 0.733 | 2.561 | 113,000 |
| OM09-10COPS-MS | 61.451 | 0.081 | 7.649 | 0.153 | 1.120 | 0.081 | 1.416 | 0.153 | 1.476 | 2.178 | 0.959 | 2.183 | – |
| *Mg-rich outcrop veins:* | | | | | | | | | | | | | |
| OM09-47C-MS | 67.905 | 0.295 | 8.666 | 0.456 | 1.237 | 0.295 | 1.604 | 0.456 | 8.553 | 7.850 | 0.188 | 7.863 | 18,000 |
| OM10-13C-MG | 67.111 | 0.187 | 31.111 | 0.800 | 1.223 | 0.187 | 5.758 | 0.800 | 18.024 | 4.782 | 0.319 | 4.848 | 33,000 |
| OM10-53C-MG | 66.747 | 0.198 | 8.312 | 0.629 | 1.216 | 0.198 | 1.538 | 0.629 | 16.680 | 3.687 | 0.092 | 3.740 | 9000 |
| OM09-91C-MS | 66.866 | 0.129 | 12.481 | 0.356 | 1.218 | 0.129 | 2.310 | 0.356 | 11.551 | 15.393 | 0.200 | 15.397 | 19,000 |
| OM10-82C-MG | 67.717 | 0.262 | – | – | 1.234 | 0.262 | – | – | 10.450 | 4.656 | – | – | – |
| OM10-84C-MG | 65.139 | 0.268 | 6.723 | 0.374 | 1.187 | 0.268 | 1.244 | 0.374 | 1.520 | 3.180 | 0.818 | 3.202 | 122,000 |
| *Mg-rich roadcut veins:* | | | | | | | | | | | | | |
| OM09-35C-MS | – | – | 5.650 | 1.435 | – | – | 1.046 | 1.435 | 0.979 | 1.934 | 1.068 | 2.408 | – |
| OM09-55C-MS | 6.630 | 0.440 | 32.800 | 0.785 | 1.044 | 0.440 | 6.071 | 0.785 | 6.351 | 3.153 | 0.956 | 3.250 | 256,000 |
| OM09-57C-MS | 31.344 | 0.109 | 164.870 | 0.151 | 1.010 | 0.109 | 30.515 | 0.151 | 31.019 | 2.055 | 0.984 | 2.061 | >375,000 |
| OM09-58C-MS | 54.751 | 0.085 | – | – | 0.998 | 0.085 | – | – | 272.445 | 3.121 | – | – | – |
| OM10-52C-MG | 61.609 | 0.377 | 4.506 | 0.428 | 1.123 | 0.377 | 0.834 | 0.428 | 0.541 | 6.701 | 1.542 | 6.715 | Not determinable |
| *Sediments:* | | | | | | | | | | | | | |
| OM09-8S-MS | 56.637 | 0.067 | 28.178 | 0.075 | 1.032 | 0.067 | 5.215 | 0.075 | 5.352 | 3.162 | 0.975 | 3.163 | – |
| OM09-12S-MS | 60.501 | 0.057 | 8.621 | 0.063 | 1.102 | 0.057 | 1.596 | 0.063 | 2.093 | 7.724 | 0.762 | 7.724 | – |
| *Carbonate standard:* | | | | | | | | | | | | | |
| JCp-1 | *63.002* | *0.097* | *6.965* | *0.849* | *1.148* | *0.097* | *1.289* | *0.849* | *164.831* | *4.173* | *0.008* | *4.259* | |
| | *62.943* | *0.080* | *7.016* | *0.430* | *1.148* | *0.080* | *1.299* | *0.430* | *165.235* | *2.740* | *0.008* | *2.773* | |
| | *63.017* | *0.075* | *6.898* | *0.368* | *1.148* | *0.075* | *1.277* | *0.368* | *164.308* | *2.380* | *0.008* | *2.408* | |
| | *62.899* | *0.048* | *7.107* | *0.420* | *1.146* | *0.048* | *1.315* | *0.420* | *148.854* | *3.809* | *0.009* | *3.832* | |
| | **62.965** | **0.075** | **6.997** | **0.517** | **1.148** | **0.075** | **1.295** | **0.517** | **160.807** | **3.275** | **0.008** | **3.318** | |

( ) Denotes activity. Activity ratios calculated using: $\lambda_{230} = 9.158 \times 10^{-6}$ years$^{-1}$ (Cheng et al., 2000); $\lambda_{232} = 4.948 \times 10^{-11}$ years$^{-1}$ (Le Roux and Glendenin, 1963); $\lambda_{234} = 2.8263 \times 10^{-6}$ years$^{-1}$ (Cheng et al., 2000); and, $\lambda_{238} = 1.551 \times 10^{-10}$ years$^{-1}$; (Jaffey et al., 1971).
Errors for activity ratios include uncertainties in spike calibrations for $^{232}$Th and $^{238}$U concentrations, in run measurement error for $^{230}$Th/$^{232}$Th, and in the standards against which instrument measurements were calibrated. Errors do not include uncertainties in $\lambda_{238}$ (0.07%), $\lambda_{232}$ (0.5%), $\lambda_{230}$ (0.3%), or $\lambda_{234}$ (0.1%).

Many of the Samail carbonates are out of equilibrium with respect to ($^{230}$Th/$^{238}$U) (Fig. 5). Samples with ($^{230}$Th/$^{238}$U) = 1 plot on the equiline, indicating isotopic equilibrium. Four of the Mg-rich carbonate outcrop veins, two of the travertine terraces, and the travertine vein have ($^{230}$Th/$^{238}$U) < 1 and thus have $^{238}$U excesses. One travertine terrace sample, the two travertine pseudospeleothems, the two recently-formed travertine precipitates, one of the Mg-rich carbonate outcrop vein samples, four Mg-rich carbonate roadcut vein samples, and the two sediment samples fall very close to the equiline.

Many of the Samail carbonates are also out of equilibrium with respect to ($^{234}$U/$^{238}$U) (Fig. 6). The travertine terrace samples, recently-formed travertine precipitates, and travertine pseudospeleothems all have $^{234}$U excesses with ($^{234}$U/$^{238}$U) values ranging from 1.118 to 1.255. However, the travertine vein sample plots on the other side of the equiline with a ($^{234}$U/$^{238}$U) value of 0.832, which may indicate that the hyperalkaline Type II fluids from which this sample was precipitated reacted with material that has low $^{234}$U/$^{238}$U due to prior water–rock interaction. The Mg-rich carbonate outcrop vein samples have a fairly narrow range of ($^{234}$U/$^{238}$U) values of 1.187 to 1.237. The Mg-rich carbonate roadcut vein samples have lower ($^{234}$U/$^{238}$U) values than the outcrop vein samples, ranging from 0.998 to 1.123. Two of the roadcut vein samples have near-equilibrium ($^{234}$U/$^{238}$U) values of 0.998 (Sample OM09-58C-MS) and 1.010 (Sample OM09-57C-MS). Sediment sample OM09-8S-MS plots just above the equiline with ($^{234}$U/$^{238}$U) = 1.032 while sediment sample OM09-12S-MS, which contains significant calcite that likely derives from nearby travertines, has higher ($^{234}$U/$^{238}$U) = 1.102, which approaches the values observed in the surface travertines.

There is a large range of ($^{230}$Th/$^{232}$Th) values observed in the Samail carbonates and sediments (Fig. 7). Most samples have ($^{230}$Th/$^{232}$Th) values that fall in the range of ~0 to 6. However, the Mg-rich carbonate roadcut vein sample OM09-57C-MS has ($^{230}$Th/$^{232}$Th) = 30.515.

## 5. Discussion

### 5.1. Systematics of U and Th in Samail carbonates and sediments

#### 5.1.1. Origin of variable U and Th concentrations

The travertine samples, particularly the surface travertine samples, have the highest U and Th concentrations (Fig. 4). The high U and Th concentrations of the travertines are likely a result of incorporation of a significant amount of aluminosilicate detritus. There are multiple lines of evidence that support this interpretation. First, while the higher U concentrations of the travertines could be explained by U enrichment

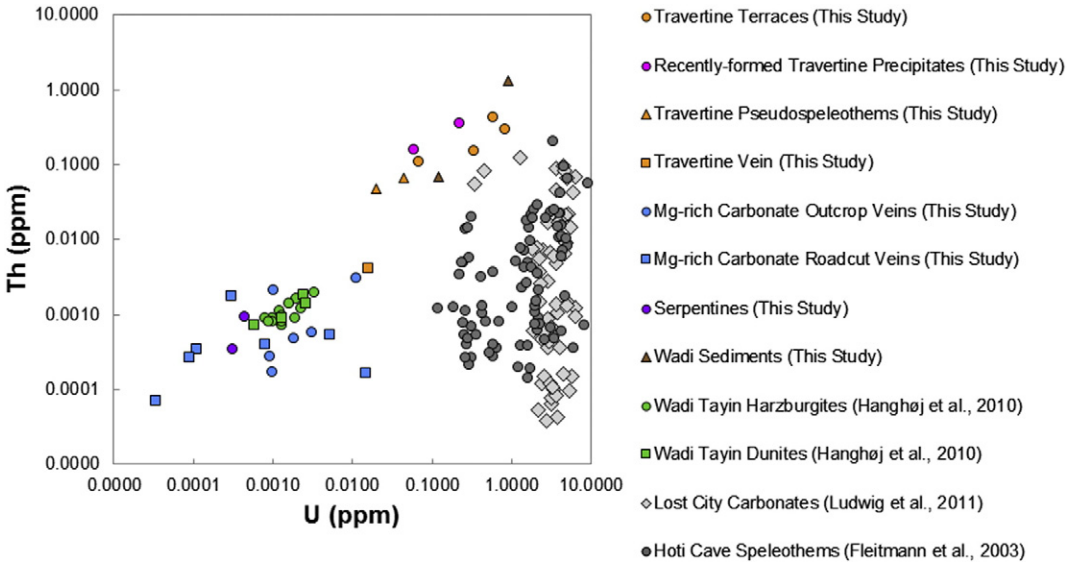


**Fig. 4.** Plot of U and Th concentrations for Samail travertines (orange circles for travertine terraces, pink circles for recently-formed travertine precipitates, orange triangles for travertine pseudospeleothems, and an orange square for the travertine vein), Mg-rich carbonate veins (blue circles for Mg-rich carbonate outcrop veins and blue squares for Mg-rich carbonate roadcut veins), serpentine mineral separates from carbonate-serpentine veins (purple circles), and wadi sediments (brown triangles). Note that both axes have a log scale. Shown for reference are U and Th concentrations for harzburgites (green circles) and dunites (green squares) from Wadi Tayin, a massif in the southern part of the Samail Ophiolite (data from Hanhøj et al., 2010); for carbonates formed at Lost City, a hydrothermal site located in peridotite ~15 km off-axis of the Mid-Atlantic Ridge (data from Ludwig et al., 2011); and for speleothems from Hoti Cave, which is located in Cretaceous age Natih limestone in northern Oman (data from Fleitmann et al., 2003).

in fluids due to low water/rock ratios, the Th concentrations can only be explained by the incorporation of detritus since Th is insoluble under almost all conditions and is believed to be insoluble in both the Type I and the Type II waters flowing through Samail peridotite (e.g. Langmuir and Herman, 1980; Porcelli and Swarzeneski, 2003). Second, light acid leaches of travertine samples (see Supplementary Information) leave behind significant aluminosilicate detritus, which has higher U and Th concentrations than the carbonate material dissolved during the light acid leach. In contrast, most of the Mg-rich carbonate vein samples do not leave behind significant aluminosilicate residues after light acid leaches. Third, the U and Th concentrations of the travertine vein sample (OM09-84C-MS), which formed in the subsurface and likely incorporated less detritus, are lower than the other travertines. Finally, the travertine samples have U and Th concentrations that are comparable to the wadi sediments, which are likely sources of detritus.

Since the travertine samples incorporate significant detritus, constraining the composition of this component is essential to correct for detrital Th in the $^{230}$Th age calculations. While fragments of serpentine and altered peridotite are observed in the travertines, these cannot be the only sources of detritus in the travertine samples because the travertine terrace samples have U and Th concentrations that are much higher than those measured in serpentine and partially serpentinized peridotites (Fig. 4; peridotite data from Hanhøj et al., 2010). However, the two wadi sediments have U and Th concentrations that are comparable with those of the travertine terrace samples. The wadi sediments contain serpentine and enstatite, which likely originate from local peridotite bedrock (Table 1). They also contain significant modal quartz, which is most likely aeolian in origin, and significant carbonate minerals, such as calcite, dolomite, and magnesite. The magnesite likely originates from local magnesite veins in peridotite. However, the calcite and dolomite could originate from local carbonate alteration products in peridotite, such as weathered travertines, and from non-local carbonates transported by wind. For example, aeolian carbonate could originate from the Cretaceous Natih formation, which has U concentrations up to ~9 ppm (Fig. 4; Natih carbonate data from Fleitmann et al., 2003). The two pseudospeleothems also have lower U and Th concentrations than the travertine terrace samples. This is likely because the formation beneath overhangs and the fine-grained texture of these pseudospeleothems reduces the amount of detritus that they incorporate. The low U concentrations of the Mg-rich carbonate vein samples reflect the low U concentrations of the peridotites (e.g. Hanhøj et al., 2010) that are altering to form these carbonates as well as the low U concentrations in the reacting fluids (Fig. 4).

*5.1.2. Systematics of U and Th isotopes*

The Samail carbonates and sediments either have $^{238}$U excesses or fall on the equiline of the ($^{230}$Th/$^{232}$Th) versus ($^{238}$U/$^{232}$Th) plot (Fig. 5). During initial precipitation from fluids, Samail carbonates should have $^{238}$U excesses. Over time, as the $^{238}$U decay chain returns to equilibrium, the isotopic compositions of the carbonates will move toward the equiline. After approximately 375,000 years (5 times the half-life of $^{230}$Th, which equates to an uncertainty of 3% in ($^{230}$Th/$^{238}$U)), the isotopic compositions of the carbonate samples will plot on the equiline. Thus, one interpretation is that the carbonate samples which plot on or close to the equiline (five travertines, one Mg-rich carbonate outcrop vein sample, and four Mg-rich carbonate roadcut vein samples) are 375,000 years or older in age. This interpretation may be valid for the carbonate veins, which incorporate lower amounts of aluminosilicate detritus, but may not be valid for the surface travertines.

As discussed previously, the travertine samples likely contain significant aluminosilicate detritus, which explains their elevated U and Th concentrations relative to the subsurface carbonates. Therefore, travertine samples that plot near or on the ($^{230}$Th/$^{232}$Th) versus ($^{238}$U/$^{232}$Th) equiline could either: (1.) be ~375,000 years or older in age or (2.) have incorporated a significant quantity of equilibrium (or near-equilibrium) detritus that overwhelms the isotopic signature of the pure travertine. The second explanation is favored since the two recently-formed travertine precipitates, which have >modern (post-1950) $^{14}$C ages (Mervine et al., 2014), fall on the equiline. These precipitates are known to have formed very recently, so old $^{230}$Th ages for these samples can be rejected. Therefore, these samples must have incorporated significant near-equilibrium detritus, such as wadi

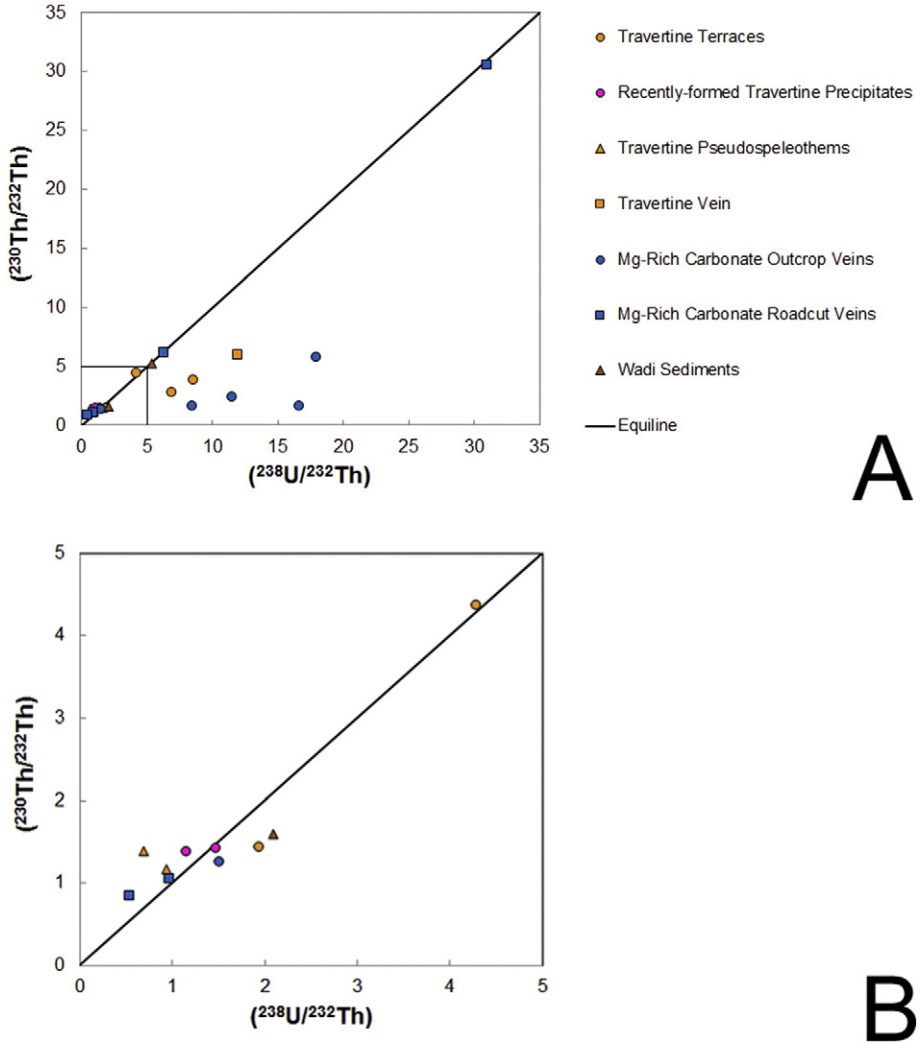


**Fig. 5.** Plot of ($^{230}$Th/$^{232}$Th) versus ($^{238}$U/$^{232}$Th) for Samail travertines, Mg-rich carbonate veins, highly altered peridotites, and wadi sediments using the same symbol scheme as Fig. 4.

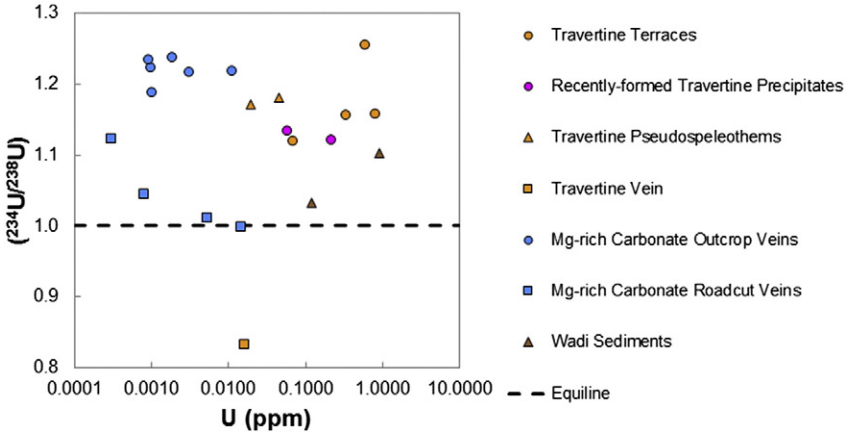


**Fig. 6.** Plot of ($^{234}$U/$^{238}$U) versus U concentration for Samail travertines, Mg-rich carbonate veins, and wadi sediments using the same symbol scheme as Fig. 4. The dashed line indicates equilibrium for ($^{234}$U/$^{238}$U).

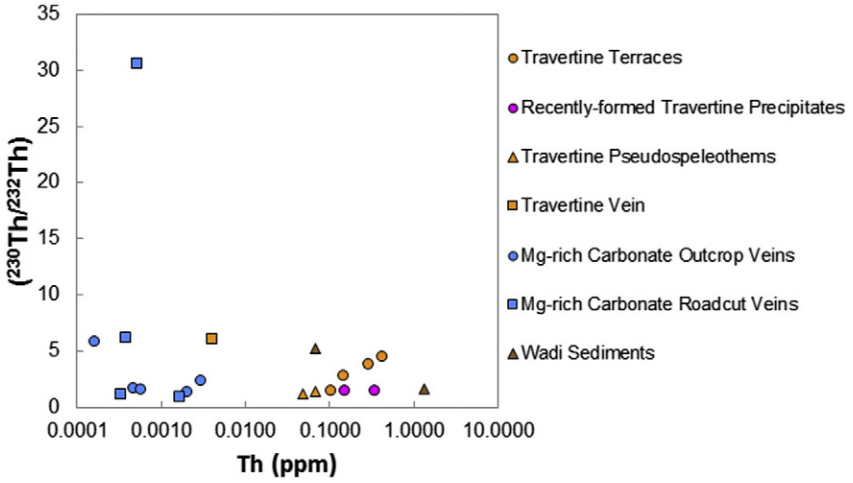


**Fig. 7.** Plot of ($^{230}$Th/$^{232}$Th) versus Th concentration for Samail travertines, Mg-rich carbonate veins, and wadi sediments using the same symbol scheme as Fig. 4.

sediments, two samples of which (OM09-8S-MS and OM09-12S-MS) fall close to the equiline. The isotopic compositions of the other travertine samples are also likely affected by the incorporation of aluminosilicate detritus. The fact that the two wadi sediment samples plot close to the equiline is not unexpected. Most aluminosilicate detritus (see the data compilation in the Supplementary Information) falls on the equiline or has slight $^{230}$Th excesses on a ($^{230}$Th/$^{232}$Th) versus ($^{238}$U/$^{232}$Th) plot. Aluminosilicate detritus rarely has $^{238}$U excesses (e.g. Szabo and Rosholt, 1982; Porcelli and Swarzneski, 2003). This is because rocks generally weather under oxidizing conditions present at and near the Earth's surface, where U is soluble and will be leached from rocks (e.g. Porcelli and Swarzneski, 2003).

### *5.2. Approaches and limitations for determining $^{230}$Th ages for Samail carbonates*

#### *5.2.1. $^{230}$Th dating of terrestrial carbonates*

$^{230}$Th dating of carbonates measures the ingrowth of $^{230}$Th from the decay of $^{238}$U and $^{234}$U incorporated into the carbonate matrix during formation. Since Th is generally highly insoluble relative to U, carbonate that forms (either through inorganic precipitation or biological processes) from marine and terrestrial waters generally contains relatively high U concentrations and low Th concentrations. This creates disequilibria in the $^{238}$U decay chain, which gradually returns to equilibrium as $^{238}$U (half-life: ~$4.47 \times 10^9$ years) and $^{234}$U (half-life: ~$2.45 \times 10^5$ years) decay to $^{230}$Th (half-life: ~$7.56 \times 10^4$ years).

$^{230}$Th dating of carbonates relies on two primary assumptions: (1.) there was no initial $^{230}$Th incorporated when the carbonate formed and (2.) there has been no loss or addition of U and Th since carbonate formation. In practice, these two assumptions are valid only for unrecrystallized, pure carbonates such as some corals and speleothems (e.g. Edwards et al., 2003; Scholz and Hoffmann, 2008). For many carbonates, these assumptions are not valid and corrections must be employed in the dating technique. If initial $^{230}$Th is present in a carbonate sample, then it may be possible to correct for this initial $^{230}$Th (e.g. Bischoff and Fitzpatrick, 1991; Luo and Ku, 1991; Kaufman, 1993; Edwards et al., 2003). Carbonates affected by open system behavior after formation, such as recrystallized corals and lacustrine carbonate with added hydrogenous U or Th, are challenging to date unless the open system behavior can be modeled (e.g. Fontes et al., 1992; Thompson et al., 2003; Villemant and Feuillet, 2003; Haase-Schramm et al., 2004).

Terrestrial carbonates are usually affected by the presence of initial $^{230}$Th and, to a lesser extent, by $^{234}$U and $^{238}$U contributed by detrital material (e.g. Bischoff and Fitzpatrick, 1991; Luo and Ku, 1991; Kaufman, 1993). Detritus incorporated into terrestrial carbonates is often fine-grained and intergrown with the carbonate, making physical separation very difficult (e.g. Ku and Liang, 1984; Bischoff and Fitzpatrick, 1991; Luo and Ku, 1991). Various approaches have been attempted over the years to account for detrital $^{230}$Th, $^{234}$U, and $^{238}$U in terrestrial carbonates to enable dating of these carbonates. Early studies (e.g. Harmon et al., 1977) attempted to separate the carbonate material from the admixed detritus by employing light acid leaches. However, numerous subsequent studies (e.g. Schwarcz and Latham, 1989; Przybylowicz et al., 1991; Bischoff and Fitzpatrick, 1991; Luo and Ku, 1991) have demonstrated that fractionation of U and Th concentrations and shifts in isotopic ratios can occur during incomplete acid leaching. Fractionation of U and Th concentrations and isotopes was also observed during partial dissolution experiments conducted on our Samail carbonate samples (see Supplementary Information). A number of studies have investigated and employed pseudoisochron methods for determining the composition of incorporated detritus (e.g. Osmond et al., 1970; Schwarcz and Lathan, 1989; Przybylowicz et al., 1991; Bischoff and Fitzpatrick, 1991; Luo and Ku, 1991). However, pseudoisochron methods are limited by the requirement of a set of coeval samples with variable detritus/carbonate ratios and thus are not suitable for dating the Samail carbonates analyzed in this study since the Samail travertines and Mg-rich carbonate veins are known to have a range of ages based on previous $^{14}$C dating (Mervine et al., 2014).

For most terrestrial carbonates, employing total sample dissolutions with corrections for detrital $^{230}$Th (and sometimes also $^{234}$U and $^{238}$U) is the most robust way to determine $^{230}$Th ages for the carbonates (e.g. Ludwig and Titterington, 1994; Edwards et al., 2003; Ludwig et al., 2011). The simplest and most commonly employed detrital correction approach uses $^{232}$Th as an indicator isotope for the $^{230}$Th correction. In this method, all $^{232}$Th is assumed to originate from detritus, and the measured ($^{232}$Th/$^{238}$U) of the terrestrial carbonate is used to weight the $^{230}$Th correction. The ($^{230}$Th/$^{232}$Th) composition of the detrital material is rarely known explicitly and is generally the largest source of uncertainty in corrected $^{230}$Th ages. Often, a Bulk Silicate Earth (BSE) value for ($^{230}$Th/$^{232}$Th) of 0.814 (calculated assuming equilibrium with ($^{238}$U/$^{232}$Th) = ($^{230}$Th/$^{232}$Th)) is assumed for the detritus (e.g. Ludwig and Titterington, 1994; Ludwig et al., 2011). Although the required assumptions are not necessarily geologically sound, assuming a BSE ($^{230}$Th/$^{232}$Th) value works for older carbonates with high U and low $^{232}$Th contents because the resulting correction is relatively insignificant, such that the assumed ($^{230}$Th/$^{232}$Th) value has a small effect on the calculated age (e.g. Bischoff and Fitzpatrick, 1991; Kaufman, 1993; Ludwig and Titterington, 1994). However, for young carbonates and for carbonates with relatively low U concentrations and high $^{232}$Th concentrations (such as the Samail carbonates), the assumed ($^{232}$Th/$^{230}$Th)

value for the detrital material has a large effect on the calculated age, and therefore the ($^{232}$Th/$^{230}$Th) value must be known explicitly in order to reliably determine corrected $^{230}$Th ages.

We have employed total dissolutions with corrections for initial $^{230}$Th in an attempt to determine $^{230}$Th ages for Samail carbonates. We have not employed corrections for detrital $^{234}$U and $^{238}$U because the initial $^{230}$Th correction has the largest influence on the age corrections. Because Samail carbonate $^{230}$Th ages are so sensitive to initial $^{230}$Th corrections and because there is not an obvious single detrital ($^{230}$Th/$^{232}$Th) value to use for the corrections, a sensitivity analysis approach has been employed to evaluate the influence of detrital $^{230}$Th on the calculated $^{230}$Th ages of the Samail carbonates.

To evaluate a reasonable range of detrital ($^{230}$Th/$^{232}$Th) values to use for the initial $^{230}$Th correction for the Samail carbonate $^{230}$Th ages, we compiled 300 literature values for ($^{230}$Th/$^{232}$Th) measured in various types (soil, saprolite, alluvium, colluvium, till, and volcanic ash) of aluminosilicate detritus (see Supplementary Information). These data were compiled from Rosholt et al. (1966), Hansen and Stout (1968), Hansen (1970), Rosholt et al. (1985), Mathieu et al. (1995), Dequincey et al. (2002), Krishnaswami et al. (2004), Dossetto et al. (2008), Pelt et al. (2008), and Ma et al. (2010). This compilation has ($^{230}$Th/$^{232}$Th) values ranging from 0.02 to 4.61 (average: 0.77, 2σ standard deviation: 0.50). While the average ($^{230}$Th/$^{232}$Th) of the compiled detritus values is fairly close to the equilibrium BSE value of 0.814, aluminosilicate detritus clearly has a wide range of ($^{230}$Th/$^{232}$Th) values. Our results show that the ($^{230}$Th/$^{232}$Th) value of the detritus incorporated into the Samail carbonates may be higher than the equilibrium BSE value. The recently-formed travertine precipitates OM09-8COPS-MS and OM09-10COPS-MS have ($^{230}$Th/$^{232}$Th) values of 1.376 and 1.416, respectively. These two precipitates are essentially zero age with respect to the half-life of $^{230}$Th (based on $^{14}$C measurements and field relations, see Mervine et al., 2014). While the ($^{230}$Th/$^{232}$Th) value of detritus incorporated in Samail carbonates is clearly spatially and temporally variable, it is important to note that the ($^{230}$Th/$^{232}$Th) values measured in the recently-formed travertine precipitates (likely formed a matter of days or weeks before collection and therefore should have minimal ingrown $^{230}$Th) are similar and provide a possible correction value to use for older travertine samples. ($^{230}$Th/$^{232}$Th) values measured in wadi sediments also provide possible values to use for initial $^{230}$Th corrections for the Samail carbonate $^{230}$Th ages. One of the wadi sediments has a ($^{230}$Th/$^{232}$Th) value of 2.093, somewhat similar to the values measured in the two recently-formed travertine precipitates. However, wadi sediment OM09-8S-MS, which consists primarily of serpentine, has a higher ($^{230}$Th/$^{232}$Th) value of 5.215. Clearly, there is significant variability in the measured ($^{230}$Th/$^{232}$Th) values of detritus that may have been incorporated into the Samail carbonates.

### 5.2.2. $^{230}$Th dating of Samail travertines

Uncorrected $^{230}$Th ages for Samail travertines are presented in Table 3. For all travertines analyzed, the uncorrected $^{230}$Th ages are significantly older than the corresponding $^{14}$C ages (Mervine et al., 2014). The low U concentrations and relatively high Th/U ratios found in the Samail travertines makes obtaining detritus corrected $^{230}$Th ages highly challenging. The travertines contain significant detrital Th, and the values of corrected $^{230}$Th ages are thus highly sensitive to the selected value of initial ($^{230}$Th/$^{232}$Th) employed in the corrections. Varying the assumed initial ($^{230}$Th/$^{232}$Th) over the range observed in wadi sediments, BSE, and our compilation of aluminosilicate detritus (see Supplementary Information) changes the corrected travertine $^{230}$Th ages by tens of thousands of years. As an example, Fig. 8 displays the effect of the selected initial ($^{230}$Th/$^{232}$Th) value on the corrected $^{230}$Th age for travertine terraces sample OM09-106C-MS-A. Similar figures for all travertine samples are presented in the Supplementary Information.

For all travertine samples, geologically plausible detrital ($^{230}$Th/$^{232}$Th) values bring the corrected $^{230}$Th ages into concordance with the $^{14}$C ages presented in Mervine et al. (2014). For example, an assumed detrital

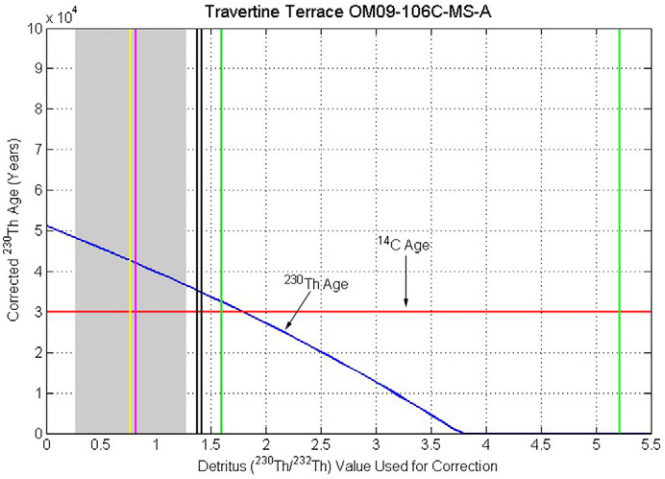


**Fig. 8.** Sensitivity analysis figure showing the effect of the selected detritus ($^{230}$Th/$^{232}$Th) correction value on the corrected $^{230}$Th age. This figure is for sample OM09-106C-MS-A, a travertine terrace sample from Wadi Uqaybah Travertine. The blue line indicates the corrected $^{230}$Th age calculated from the detritus value on the x-axis. Note that the uncorrected $^{230}$Th age plots at x = 0. For comparison, the calibrated $^{14}$C age (from Mervine et al., 2014) is plotted as the red line. The gray box indicates the 2σ range of ($^{230}$Th/$^{232}$Th) values for aluminosilicate detritus (a literature compilation of 300 values, see Supplementary Information). The vertical lines indicate possible values to use for the detritus ($^{230}$Th/$^{232}$Th) correction value: the average of the aluminosilicate detritus literature compilation (yellow line), equilibrium Bulk Silicate Earth (pink line), wadi sediments (green lines), and recently-formed travertine precipitates (black lines). The choice of the ($^{230}$Th/$^{232}$Th) correction value has a very significant impact on the determined $^{230}$Th age, which ranges from ~50,000 years to zero depending on the correction value selected. However, a ($^{230}$Th/$^{232}$Th) correction value of approximately 1.7 brings the corrected $^{230}$Th age into concordance with the $^{14}$C age.

($^{230}$Th/$^{232}$Th) value of ~1.7 produces a corrected $^{230}$Th or sample OM09-106C-MS-A that is concordant with the $^{14}$C age of 30,023 ± 235 years BP reported in Mervine et al. (2014). Unfortunately, no single detrital ($^{230}$Th/$^{232}$Th) value consistently corrects the travertine $^{230}$Th ages to the corresponding $^{14}$C ages. The different ($^{230}$Th/$^{232}$Th) corrections required for each travertine are likely a result of the observed heterogeneous nature of the detritus. Therefore, although geologically plausible ($^{230}$Th/$^{232}$Th) values can be selected for each travertine to bring the corrected $^{230}$Th age into concordance with the $^{14}$C age, the lack of a uniform ($^{230}$Th/$^{232}$Th) correction value precludes obtaining precise ages for Samail travertines using $^{230}$Th dating alone.

### 5.2.3. $^{230}$Th dating of Samail Mg-rich carbonate veins

Uncorrected $^{230}$Th ages for Mg-rich carbonate vein samples are presented in Table 3. Four out of the five Mg-rich carbonate outcrop vein samples have uncorrected $^{230}$Th ages that are younger than the corresponding $^{14}$C ages (Mervine et al., 2014). The exception is sample OM10-84C-MG, which has a $^{230}$Th age older than its $^{14}$C age. While not particularly high, the ~2 ppb Th concentration of sample OM10-84C-MG is significant relative to its low U concentration of ~1 ppb. Therefore, sample OM10-84C-MG likely contained significant initial $^{230}$Th relative to its U concentration. Furthermore, the Th/U ratio (1.995) of OM10-84C-MG is significantly higher than the other carbonate outcrop veins, which have Th/U ratios of ~0.2 to ~0.3.

Since the uncorrected $^{230}$Th ages of the Mg-rich carbonate outcrop veins are generally younger than the corresponding $^{14}$C ages, corrections for initial $^{230}$Th from detritus cannot be employed to make the two sets of ages concordant since initial $^{230}$Th corrections would make the $^{230}$Th ages even younger. Fig. 9 illustrates the effect of a range of initial $^{230}$Th corrections for Mg-rich carbonate outcrop vein OM10-13C-MG. Similar figures for all of the Mg-rich carbonate outcrop vein samples are presented in the Supplementary Information. Possibly, a detrital correction employing an unusual detritus with $^{238}$U enrichment, such as

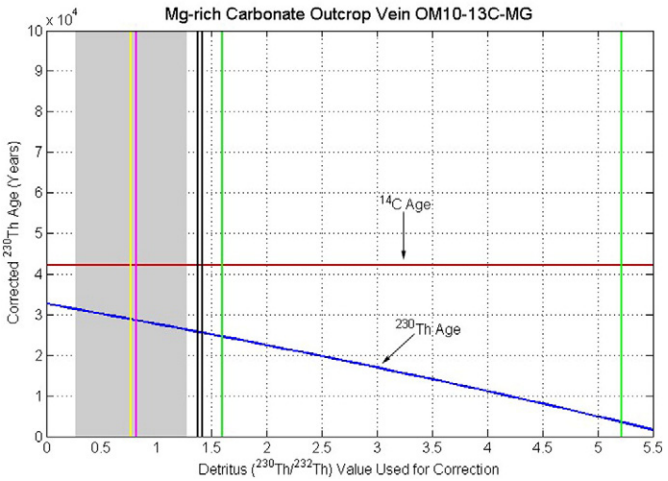


**Fig. 9.** Sensitivity analysis figure showing the effect of the selected detritus ($^{230}Th/^{232}Th$) correction value on the corrected $^{230}Th$ age. This figure is for sample OM10-13C-MG, an Mg-rich carbonate outcrop vein from Fanja Roadcut. The blue line indicates the corrected $^{230}Th$ age calculated from the detritus value on the x-axis. Note that the uncorrected $^{230}Th$ age plots at x = 0. For comparison, the calibrated $^{14}C$ age (from Mervine et al., 2014) is plotted as the red line. The gray box indicates the 2σ range of ($^{230}Th/^{232}Th$) values for aluminosilicate detritus (a literature compilation of 300 values, see Supplementary Information). The vertical lines indicate possible values to use for the detritus ($^{230}Th/^{232}Th$) correction value: the average of the aluminosilicate detritus literature compilation (yellow line), equilibrium Bulk Silicate Earth (pink line), wadi sediments (green lines), and recently-formed travertine precipitates (black lines). The choice of the ($^{230}Th/^{232}Th$) correction value has a very significant impact on the determined $^{230}Th$ age, which ranges from ~30,000 years to zero depending on the correction value selected. Since the uncorrected $^{230}Th$ age is younger than the $^{14}C$ age, no ($^{230}Th/^{232}Th$) correction value can bring the two ages into concordance.

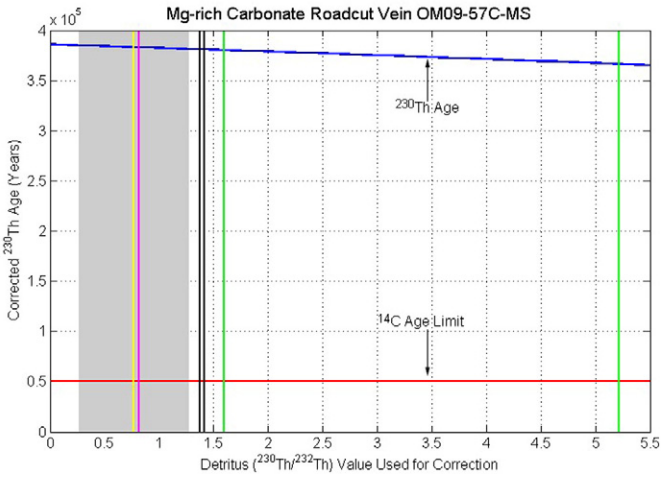


**Fig. 10.** Sensitivity analysis figure showing the effect of the selected detritus ($^{230}Th/^{232}Th$) correction value on the corrected $^{230}Th$ age. This figure is for sample OM09-57C-MS, an Mg-rich carbonate roadcut vein from Fanja Roadcut. The blue line indicates the corrected $^{230}Th$ age calculated from the detritus value on the x-axis. Note that the uncorrected $^{230}Th$ age plots at x = 0. For comparison, the calibrated $^{14}C$ age (from Mervine et al., 2014) is plotted as the red line. The gray box indicates the 2σ range of ($^{230}Th/^{232}Th$) values for aluminosilicate detritus (a literature compilation of 300 values, see Supplementary Information). The vertical lines indicate possible values to use for the detritus ($^{230}Th/^{232}Th$) correction value: average of aluminosilicate detritus literature compilation (yellow line), equilibrium Bulk Silicate Earth (pink line), wadi sediments (green lines), and recently-formed travertine precipitates (black lines). The choice of the ($^{230}Th/^{232}Th$) correction value has a minimal impact on the determined $^{230}Th$ age, which remains greater than 350,000 years. This is consistent with the $^{14}C$ dead (>50,000 years BP) age limit of this sample.

a highly altered peridotite, could be employed to make the $^{230}Th$ ages older.

There are two possible end member explanations for the discrepancies between the $^{230}Th$ and $^{14}C$ ages for the Mg-rich carbonate outcrop vein samples. The first explanation is that the $^{230}Th$ ages are correct but the $^{14}C$ ages are too old because of the incorporation of recycled, $^{14}C$ dead carbon. The second explanation is that the $^{230}Th$ ages are too young because of $^{238}U$ addition from U-bearing fluids. Essentially, hexavalent U, which is highly soluble, is being carried down from the surface by the oxidized Type I waters; this U is subsequently deposited as tetravalent U by the Type II reducing serpentinization fluids. We also note that if the carbonate outcrop veins were modified by U addition from fluid, then their $^{14}C$ ages may have also been partially or fully reset. Therefore, because of the possible effects of incorporated old carbon with no $^{14}C$ and/or open system addition of young carbon with high $^{14}C$, the $^{14}C$ ages of altered Mg-rich carbonate veins should be interpreted with caution. The $^{14}C$ ages could be affected by both types of end member open system behavior, including multiple generations of open system behavior. The uncorrected $^{230}Th$ ages for the Mg-rich carbonate roadcut vein samples are significantly older than the uncorrected $^{230}Th$ ages for the Mg-rich carbonate outcrop vein samples. The roadcut vein samples have ($^{230}Th/^{238}U$) values approaching equilibrium. Mg-rich carbonate roadcut vein samples OM09-35C-MS, OM09-55C-MS, and OM09-57C-MS have ($^{230}Th/^{238}U$) values of 1.068, 0.956, and 0.984, respectively. Furthermore, Mg-rich roadcut vein samples OM09-57C-MS, and OM09-58C-MS have near-equilibrium ($^{234}U/^{238}U$) values of 1.010, and 0.998, respectively. These four Mg-rich carbonate roadcut vein samples are $^{14}C$ dead, suggesting that their ages are >50,000 years BP (Mervine et al., 2014). Thus, the older $^{230}Th$ ages suggested by the near-equilibrium ($^{230}Th/^{238}U$) and ($^{234}U/^{238}U$) values are consistent with the $^{14}C$ data. As shown in Fig. 10, applying a wide range of ($^{230}Th/^{232}Th$) detrital values for an initial $^{230}Th$ correction does not affect the $^{230}Th$ age of sample OM09-57C-MS significantly. Unfortunately, Th isotopes could not be measured in Sample OM09-58C-MS due to its low Th concentration. Given the long half-life of $^{234}U$ ($t_{1/2} = 2.45 \times 10^5$ years), the near-equilibrium ($^{234}U/^{238}U$) values for these two veins suggest that these samples are several hundred thousand years old. An alternate explanation would be that these samples started out with ($^{234}U/^{238}U$) in equilibrium. However, we consider this an unlikely initial condition given: (1.) the extent of ($^{234}U/^{238}U$) disequilibria observed in the other Mg-carbonate samples (Fig. 6); (2.) that most crustal waters (seemingly including those forming these veins, see Fig. 6) are enriched in $^{234}U$ relative to $^{238}U$, because of well-documented alpha recoil and lattice damage effects (Porcelli and Swarzneski, 2003); and (3.) these inferred old ages are consistent with other isotopic characteristics which also indicate that they are old, namely equilibrium ($^{230}Th/^{238}U$) and $^{14}C$ dead radiocarbon measurements.

Mg-rich carbonate roadcut vein sample OM10-52C-MG has a ($^{230}Th/^{238}U$) value of 1.542, which is a value that cannot be reached through closed-system $^{238}U$ decay and $^{230}Th$ ingrowth. Therefore, no $^{230}Th$ age can be determined for this sample. The high ($^{230}Th/^{238}U$) value of this sample is likely explained by high detrital $^{230}Th$ since it has a very high Th/U ratio of 5.6.

### 5.3. Implications for natural rates of carbonate formation in Samail peridotite

The determination of precise $^{230}Th$ ages for Samail carbonates is limited by large and uncertain initial $^{230}Th$ corrections. Nevertheless, the U and Th systematics and the age limits from the $^{230}Th$ dating attempts permit further refinement of previous estimates of natural rates of carbon sequestration in Samail carbonates (Kelemen and Matter, 2008; Kelemen et al., 2011; Mervine et al., 2014).

The fact that geologically reasonable initial $^{230}Th$ corrections bring $^{230}Th$ and $^{14}C$ ages for travertines into concordance further supports prior inferences that $^{14}C$ dating of travertines is generally reliable and these ages can be interpreted as formation ages. This places additional

confidence on the estimates, based on $^{14}C$ dating, that travertine precipitation rates are ~0.1 to ~0.3 mm/year and that travertines in the Samail Ophiolite are sequestering a maximum of ~1 to 3 × $10^6$ kg $CO_2$/year (Mervine et al., 2014).

U and Th systematics and $^{230}Th$ ages for the Mg-rich carbonate vein samples also provide further evidence that there are multiple generations of Mg-rich carbonate veins in the peridotite subsurface. The fact that the Mg-rich carbonate outcrop veins have $^{230}Th$ ages younger than the corresponding $^{14}C$ ages suggests that these carbonate veins may have been altered by U-bearing fluids within the last 375,000 years. The lack of concordance between $^{230}Th$ and $^{14}C$ ages for the Mg-rich carbonate outcrop veins also suggests that these carbonate veins may have been affected by open system behavior, most likely dissolution and re-precipitation of previous generations of carbonate veins. Such open system behavior may have perturbed both the $^{14}C$ and $^{230}Th$ ages for Mg-rich carbonate veins.

The near-equilibrium ($^{230}Th/^{238}U$) and ($^{234}U/^{238}U$) values measured in the less weathered, $^{14}C$ dead, Mg-rich carbonate roadcut veins suggest that, at certain exposures such as Fanja Roadcut, there may be much older (possibly older than 1 million years, based on the equilibrium $^{234}U/^{238}U$ values) generations of Mg-rich carbonate veins preserved at these localities. Therefore, carbonate vein formation in the peridotite layer of the Samail Ophiolite has likely been ongoing for at least the past 50,000 years and possibly for a much longer time. Hence, sensitivity analysis, such as that presented in Mervine et al. (2014), that considers the impact of multiple generations of carbonate vein formation on the estimated rate of $CO_2$ sequestration in subsurface carbonate veins is essential since there is no single "average" carbonate vein age. The sensitivity analysis presented in Mervine et al. (2014) indicates that ongoing Mg-rich carbonate vein formation in the peridotite layer of the Samail Ophiolite sequesters on the order of $10^7$ kg of $CO_2$ per year, consistent with less well-constrained, previous estimates (Kelemen and Matter, 2008; Kelemen et al., 2011).

### 5.4. Implications for U–Th disequilibria dating of terrestrial Quaternary carbonates

The results of this study indicate that U–Th disequilibria dating of Quaternary carbonate alteration minerals formed in ophiolite peridotites is highly challenging, due to low U concentrations, high Th/U ratios, and the open system nature of some of the carbonates. This study concurs with previous investigations (e.g. Schwarcz and Latham, 1989; Przybylowicz et al., 1991; Kaufman, 1993) that partial dissolution approaches are not recommended for U–Th disequilibria dating of terrestrial carbonates, due to fractionation of U and Th concentrations and isotopic values. Unfortunately, U–Th disequilibria dating approaches employing total dissolutions with detrital corrections (e.g. Kaufman, 1993; Ludwig et al., 2011) were also challenging to implement. The travertine samples analyzed in this study contained high amounts of detritus, which appears to be heterogeneous in nature with no single ($^{230}Th/^{232}Th$) correction value that can be employed to determine reliable ages that are comparable with previously obtained $^{14}C$ ages. The very low U concentrations of the subsurface carbonate vein samples required the dissolution of large amounts of carbonate material. In addition, although the subsurface carbonate vein samples contained significantly less detritus than the travertines, the very low U concentrations of these samples means that the age calculations remain highly sensitive to detrital corrections. Furthermore, combined analysis of U–Th disequilibria systematics and $^{14}C$ dating indicates that some of the subsurface carbonate veins have been affected by open system behavior. In this case, neither the U–Th disequilibria nor the $^{14}C$ ages can be considered reliable. However, investigation of U–Th systematics was a useful tool for identifying this open system behavior, even though U–Th disequilibria ages could not be determined.

The determination of precise U–Th disequilibria ages for carbonate alteration minerals formed in peridotites with low U concentrations is likely to remain highly challenging. Thus, other dating techniques, such as (U–Th)/He dating of magnetite, an alteration product formed in association with serpentine minerals and also carbonate (e.g. Hernandez Goldstein et al., 2014), may have to be explored to better understand timescales of natural peridotite alteration. However, U–Th disequilibria dating techniques should remain useful for dating carbonate alteration products in seafloor peridotites since these carbonates commonly have higher U concentrations due to U contributions from seawater (e.g. Ludwig et al., 2011).

U–Th disequilibria dating techniques, as well as U–Pb dating techniques, could also potentially prove useful for dating carbonate alteration products that form in other types of igneous rocks (e.g. basalts, gabbros, kimberlites) that have higher U concentrations. As an example, these techniques could potentially be used to determine ages of kimberlite carbonates. Although kimberlites, like peridotites, are ultramafic rocks comprised largely of olivine (as a primary mineral and as macrocrysts) and pyroxene (as xenocrysts), they have significantly higher U concentrations (ppm level) than peridotites since they are formed through low degrees of mantle melting (e.g. Mitchell, 1986). Potentially, the U–Th disequilibria and U–Pb dating techniques could help kimberlite geologists better understand which carbonates are primary (i.e. magmatic) and which are secondary (i.e. formed through alteration processes). However, some work will be required to better understand the distribution of U and Th in kimberlite minerals. For example, U will most likely be concentrated in minerals such as apatite and perovskite (e.g. Mitchell, 1986), and magmatic carbonates could potentially contain significant Th. Although challenges remain and these must be properly understood and accounted for, U–Th disequilibria dating nevertheless remains an important tool to consider for the dating of several types of terrestrial carbonates, including some types of carbonate alteration minerals.

## 6. Conclusions

This study highlights the difficulties of using $^{238}U$–$^{234}U$–$^{230}Th$ disequilibria measurements to determine ages for carbonate alteration minerals formed in peridotite. Our efforts to use $^{238}U$–$^{234}U$–$^{230}Th$ measurements to date both travertines and Mg-rich carbonate veins in the peridotite layer of the Samail Ophiolite show:

(1.) Samail carbonates have extremely low U and Th concentrations, which reflect the low U and Th concentrations found in Samail peridotites and associated groundwaters. The higher U and Th concentrations observed in surface travertine terraces relative to subsurface carbonate veins likely result from the higher amounts of aluminosilicate detritus incorporated into these surface samples. The low U concentrations and relatively high Th/U ratios found in Samail carbonates make obtaining $^{230}Th$ ages for these samples highly challenging.

(2.) The ($^{238}U/^{232}Th$) versus ($^{230}Th/^{232}Th$) pseudoisochron method cannot be rigorously used to date the Samail carbonate alteration minerals. This method requires coeval samples, and the Samail travertines and Mg-rich carbonate veins have a large range of $^{14}C$ ages (Mervine et al., 2014) relative to the half-life of $^{230}Th$. The travertine ages in particular can vary by thousands of years over short distances (mm to cm scale).

(3.) Partial dissolution experiments to separate the fine-grained, inter-grown aluminosilicate detritus from the carbonate show that even light acid leaching significantly perturbs the U/Th and ($^{230}Th/^{232}Th$) of the dissolved carbonates. These isotopic and elemental perturbations are from partial leaching of the fine-grained silicates. Because this leached out silicate contribution cannot be explicitly quantified, partial dissolution is not a viable method for dating the carbonate.

(4.) For the travertines, because of the issues outlined in conclusions 1, 2 and 3 above, the most viable method for obtaining reliable

$^{230}$Th ages is total dissolution and correcting for the $^{230}$Th contributed by the detritus. Because these travertines contain significant initial $^{230}$Th from detritus, the values of the ages obtained through correction for $^{230}$Th from detritus are highly sensitive to the selected value of initial ($^{230}$Th/$^{232}$Th) used in the correction. For all travertine samples, varying the initial ($^{230}$Th/$^{232}$Th) used in the correction changes the ages of the travertines by tens of thousands of years. However, geologically plausible initial ($^{230}$Th/$^{232}$Th) values correct the travertine $^{230}$Th ages to the corresponding $^{14}$C ages (Mervine et al., 2014). This age concordance suggests that the travertines are closed systems, adding a level of credence to the reliability of the $^{14}$C ages (Mervine et al., 2014) and even the U-series ages (albeit with large uncertainties) obtained in this study.

(5.) Most Mg-rich carbonate veins from outcrops on the natural peridotite weathering surface have uncorrected $^{230}$Th ages that are younger than the corresponding $^{14}$C ages. The lack of concordance between $^{230}$Th and $^{14}$C ages for the Mg-rich carbonate outcrop veins indicates that these carbonate veins have been affected by open system behavior, most likely dissolution and re-precipitation of previous generations of carbonate veins and old carbon. Alternatively, the continuous addition of $^{238}$U from fluids would make the $^{230}$Th ages too young. If the carbonate outcrop veins were modified by U addition from fluid, then their $^{14}$C ages may have also been partially or fully re-set and thus the $^{14}$C ages of altered Mg-rich carbonate veins should be interpreted with caution.

(6.) Some $^{14}$C dead, Mg-rich carbonate veins from roadcuts have ($^{230}$Th/$^{238}$U) and ($^{234}$U/$^{238}$U) values approaching equilibrium and are likely ≫ 375,000 years in age. The variable (young and old) ages for the Mg-rich carbonate veins support the conclusions of $^{14}$C dating (Clark and Fontes, 1990; Clark et al., 1992; Kelemen and Matter, 2008; Kelemen et al., 2011; Mervine et al., 2014) that carbonation of the peridotite layer of the Samail Ophiolite is an ongoing process and that there are multiple generations of subsurface carbonate vein formation that must be considered when estimating natural rates of $CO_2$ sequestration in the peridotite layer of the Samail Ophiolite.

(7.) Overall, this study has shown that using $^{238}$U–$^{234}$U–$^{230}$Th disequilibria measurements to determine ages for carbonate alteration minerals formed in peridotite is challenging due to the generally low U concentrations and high Th/U ratios of the carbonates. In particular, further development is required to better account for the isotopic signature of admixed aluminosilicate detritus. Nevertheless, this study has shown that investigation of U–Th systematics is a useful tool for identifying open system behavior in some carbonate alteration minerals, even when precise U–Th disequilibria ages cannot be determined. In addition, U–Th disequilibria dating techniques remain useful for dating carbonate alteration products in seafloor peridotites since these carbonates commonly have higher U concentrations due to U contributions from seawater (e.g. Ludwig et al., 2011). U–Th disequilibria dating techniques could also potentially prove useful for dating carbonate alteration products that form in other types of igneous rocks that have higher U concentrations, such as basalts and kimberlites.

## Acknowledgments

Ali Al-Rajhi, Ministry of Commerce and Industry, Sultanate of Oman, and Sobhi Nasir, Sultan Qaboos University, are thanked for logistical support during field seasons. The Oman field teams are thanked for assistance with fieldwork and for scientific discussions. Jerzy Blusztajn is thanked for mentorship and assistance in the laboratory, and Vera Pavel is thanked for assistance with MATLAB programming. Jürg Matter is thanked for providing the water samples. This research was funded by the National Science Foundation grants EAR-1049281 and EAR-1049905, the Deep Ocean Exploration Institute at Woods Hole Oceanographic Institution, the Academic Programs Office at Woods Hole Oceanographic Institution, the Mellon Foundation, a Research Initiative in Science and Engineering Grant from Columbia University to Peter Kelemen and Jürg Matter, and Peter Kelemen's Arthur D. Storke Chair at Columbia University. Lucy McGee and an anonymous reviewer are thanked for comments which improved the paper. David Hilton is thanked for editorial handling.

## Appendix A. Supplementary data

Supplementary data to this article can be found online at http://dx.doi.org/10.1016/j.chemgeo.2015.07.023.

## References

Ball, L., Sims, K.W.W., Schwieters, J., 2008. Measurement of $^{234}$U/$^{238}$U and $^{230}$Th/$^{232}$Th in volcanic rocks using the Neptune MC-ICP-MS. J. Anal. At. Spectrom. 23, 173–180.
Barnes, I., O'Neil, J.R., 1969. The relationship between fluids in some fresh Alpine type ultramafics and possible modern serpentinization, Western United States. Geol. Soc. Am. Bull. 80, 1947–1960.
Barnes, I., O'Neil, J.R., 1971. Calcium-magnesium carbonate solid solutions from Holocene conglomerate cements and travertines in the Coast Range of California. Geochim. Cosmochim. Acta 35, 699–718.
Barnes, I., LaMarche, V.C., Himmelberg, G., 1967. Geochemical evidence of present day serpentinization. Science 156, 830–832.
Barnes, I., O'Neil, J.R., Trescases, J.J., 1978. Present-day serpentinization in New Caledonia, Oman, and Yugoslavia. Geochim. Cosmochim. Acta 42, 144–145.
Beinlich, A., Austrheim, H., 2012. *In situ* sequestration of atmospheric $CO_2$ at low temperature and surface cracking of serpentinized peridotite in mine shafts. Chem. Geol. 332–333, 32–44.
Bischoff, J.L., Fitzpatrick, J.A., 1991. U-series dating of impure carbonates: an isochron technique using total-sample dissolution. Geochim. Cosmochim. Acta 55, 543–554.
Bodinier, J.-L., Godard, M., 2014. Orogenic, ophiolitic, and abyssal peridotites. In: Holland, H., Turekian, K. (Eds.), Treatise on Geochemistry, 2nd Ed., pp. 103–166.
Bruni, J., Canepa, M., Chiodini, G., Cioni, R., Cipolli, F., Longinelli, A., Marini, L., Ottonello, G., Zuccolini, M.V., 2002. Irreversible water–rock mass transfer accompanying the generation of the neutral, Mg–$HCO_3$ and high-pH, Ca–OH spring waters of the Genova province, Italy. Appl. Geochem. 17, 455–474.
Chavagnac, V., Ceuleneer, G., Monnin, C., Lansac, B., Hoareau, G., Boulart, C., 2013a. Mineralogical assemblages forming at hyperalkaline warm springs hosted on ultramafic rocks: a case study of Oman and Ligurian ophiolites. Geochem. Geophys. Geosyst. 14, 2474–2495.
Chavagnac, V., Monnin, C., Ceuleneer, G., Boulart, C., Hoareau, G., 2013b. Characterization of hyperalkaline fluids produced by low-temperature serpentinization of mantle peridotites in the Oman and Ligurian ophiolites. Geochem. Geophys. Geosyst. 14, 2496–2522.
Cheng, H., Edwards, R.L., Hoff, J., Gallup, C.D., Richards, D.A., Asmerom, Y., 2000. The half-lives of uranium-234 and thorium-230. Chem. Geol. 169, 17–33.
Cipolli, F., Gambardella, B., Marini, L., Otonello, G., Zuccolini, M.V., 2004. Geochemistry of high-pH waters from serpentinites of the Gruppo di Voltri (Genova, Italy) and reaction path modeling of $CO_2$ sequestration in serpentine aquifers. Appl. Geochem. 19, 787–802.
Clark, I.D., Fontes, J.-C., 1990. Paleoclimate reconstruction in northern Oman based on carbonate from hyperalkaline groundwaters. Quat. Res. 33, 320–336.
Clark, I.D., Fontes, J.-C., Fritz, P., 1992. Stable isotope disequilibria in travertine from high pH waters: Laboratory investigations and field observations from Oman. Geochim. Cosmochim. Acta 56, 2041–2050.
Coleman, R.G., 1977. Ophiolites. Springer-Verlag, New York.
Coleman, R.G., 1981. Tectonic setting for ophiolite obduction in Oman. J. Geophys. Res. 86, 2497–2508.
Dequincey, O., Chabaux, F., Clauer, N., Sigmarsson, O., Liewig, N., Leprun, J.-C., 2002. Chemical mobilizations in laterites: evidence from trace elements and $^{238}$U–$^{234}$U–$^{230}$Th disequilibria. Geochim. Cosmochim. Acta 66, 1197–1210.
Dewandel, B., Lachassagne, P., Bakalowicz, M., Weng, P., Al-Malki, A., 2003. Evaluation of aquifer thickness by analyzing recession hydrographs: application to the Oman ophiolite hard-rock aquifer. J. Hydrol. 274, 248–269.
Dewandel, B., Lachassagne, P., Qatan, A., 2004. Spatial measurements of stream baseflow, a relevant method for aquifer characterization and permeability evaluation: application to a hard rock aquifer, Oman ophiolite. Hydrol. Process. 18, 3391–3400.
Dewandel, B., Lachassagne, P., Boudier, F., Al-Hattali, S., Ladouche, B., Pinault, J.-L., Al-Suleimani, Z., 2005. A conceptual and hydrogeological model of ophiolite hard-rock aquifers in Oman based on a multiscale and multidisciplinary approach. Hydrogeol. J. 13, 708–726.
Dossetto, A., Turner, S.P., Chappell, J., 2008. The evolution of weathering profiles through time: new insights from uranium-series isotopes. Earth Planet. Sci. Lett. 274, 359–371.

Edwards, L.R., Chen, J.H., Wasserburg, G.J., 1986. $^{238}U$–$^{234}U$–$^{230}Th$–$^{232}Th$ systematics and the precise measurement of time over the past 500,000 years. Earth Planet. Sci. Lett. 81, 175–192.

Edwards, L.R., Gallup, C., Cheng, H., 2003. Uranium-series dating of marine and lacustrine carbonates. In: Bourdon, B., Henderson, G.M., Lundstrom, C.C., Turner, S.P. (Eds.), Uranium-Series Geochemistry. Reviews in Mineralogy and Geochemistry 52, pp. 363–406.

Ferry, J.M., 1995. Fluid-flow during contact-metamorphism of ophicarbonate rocks in the Bergell-Aureole, Val-Malenco, Italian Alps. J. Petrol. 36, 1039–1053.

Fleitmann, D., Burns, S.J., Neff, U., Mangini, A., Matter, A., 2003. Changing moisture sources over the last 350,000 years in northern Oman from fluid inclusion evidence in speleothems. Quat. Res. 60, 223–232.

Fontes, J.-C., Andrews, J.N., Causse, C., Gibert, E., 1992. A comparison of radiocarbon and U/Th ages on continental carbonates. Radiocarbon 34, 602–610.

Früh-Green, G.L., Kelley, D.S., Bernasconi, S.M., Karson, J.A., Ludwig, K.A., Butterfield, D.A., Boschi, C., Proskurowski, G., 2003. 30,000 years of hydrothermal activity at the Lost City vent field. Science 301, 495–498.

Glennie, K.W., Bouef, M.G.A., Hughes-Clarke, M.W., Moody-Stuart, M., Pilaar, W.F.H., Reinhart, B.M., 1973. Late Cretaceous nappes in the Oman mountains and their geological evolution. Am. Assoc. Pet. Geol. Bull. 57, 5–27.

Glennie, K.W., Bouef, M.G.A., Hughes-Clarke, M.W., Moody-Stuart, M., Pilaar, W.F.H., Reinhart, B.M., 1974. Geology of the Oman Mountains. Part I: text. Part II: tables and illustrations. Part III: enclosures. Verhandelingen van het Koniklijk Nederlands Geologisch Mijnbouwkundig Genootschap 31 p. 423.

Haase-Schramm, A., Goldstein, S.L., Stein, M., 2004. U–Th dating of Lake Lisan (late Pleistocene Dead Sea) aragonite and implications for glacial East Mediterranean climate change. Geochim. Cosmochim. Acta 68, 985–1005.

Hanhøj, K., Kelemen, P.B., Hassler, D., Godard, M., 2010. Composition and genesis of depleted mantle peridotites from the Wadi Tayin massif, Oman Ophiolite; major and trace element geochemistry, and Os isotope and PGE systematics. J. Petrol. 51, 201–227.

Hansen, R.O., 1970. Radioactivity of a California terrace soil. Soil Sci. 110, 31–36.

Hansen, R.O., Stout, P.R., 1968. Isotopic distributions of uranium and thorium in soils. Soil Sci. 105, 44–50.

Harmon, S.R., Ford, D.C., Schwarcz, H.P., 1977. Interglacial chronology of the Rocky and Mackenzie Mountains based upon $^{230}Th$–$^{234}U$ dating of calcite speleothems. Can. J. Earth Sci. 14, 2543–2552.

Harrison, A.L., Power, I.M., Dipple, G.M., 2013. Accelerated carbonation of brucite in mine tailings for carbon sequestration. Environ. Sci. Technol. 47, 126–134.

Hellstrom, J., Pickering, R., 2015. Recent advances and future prospects of the U–Th and U–Pb chronometers applicable to archaeology. J. Archaeol. Sci. 56, 32–40.

Hernandez Goldstein, E., Stockli, D., Ketcham, R., Seman, S., 2014. (U–Th)/He dating of magnetites in serpentinites (Abstract). Goldschmidt Geochemistry Conference, Sacramento, California.

Jaffey, A.H., Flynn, K.F., Glendenin, L.E., Bentley, W.C., Essling, A.M., 1971. Precision measurement of half-lives and specific activities of $^{235}U$ and $^{238}U$. Phys. Rev. C 4, 1889–1906.

Kaufman, A., 1993. An evaluation of several methods for determining $^{230}Th/U$ ages in impure carbonates. Geochim. Cosmochim. Acta 57, 2303–2317.

Kelemen, P.B., Matter, J.M., 2008. *In situ* carbonation of peridotite for $CO_2$ storage. Proc. Natl. Acad. Sci. 105, 17295–17300.

Kelemen, P.B., Matter, J.M., Streit, E.E., Rudge, J.F., Curry, W.B., Blusztajn, J., 2011. Rates and mechanisms of mineral carbonation in peridotite: natural processes and recipes for enhanced, *in situ* $CO_2$ capture and storage. Annu. Rev. Earth Planet. Sci. 39, 545–576.

Kelley, D.S., Karson, J.A., Blackman, D.K., Früh-Green, G.L., Butterfield, D.A., Lilley, M.D., Olson, E.J., Schrenk, M.O., Roe, K.K., Lebon, G.T., Rivizzigo, P., 2001. An off-axis hydrothermal vent field near the Mid-Atlantic Ridge at 30 degrees N. Nature 412, 145–149.

Kelley, D.S., Karson, J.A., Früh-Green, G.L., Yoerger, D.R., Shank, T.M., Butterfield, D.A., Hayes, J.M., Schrenk, M.O., Olson, E.J., Proskurowski, G., Jakuba, M., Bradley, A., Larson, B., Ludwig, K., Glickson, D., Buckman, K., Bradley, A.S., Brazelton, W.J., Roe, K., Elend, M.J., Delacour, A., Bernasconi, S.M., Lilley, M.D., Baross, J.A., Summons, R.E., Sylvia, S.P., 2005. A serpentinite-hosted ecosystem: the Lost City hydrothermal field. Science 307, 1428–1434.

Krishnaswami, S., Williams, G.A., Graustein, W.C., Turekian, K.K., 2004. The effect of weathering regime on uranium decay series and osmium in two soil profiles. Geochem. J. 38, 651–660.

Ku, T.-L., Liang, Z.-C., 1984. The dating of impure carbonates with decay-series isotopes. Nucl. Instrum. Methods Phys. Res. 223, 563–571.

Lackner, K.S., 2002. Carbonate chemistry for sequestering fossil carbon. Annu. Rev. Energy Environ. 27, 193–232.

Lackner, K.S., Wendt, C.H., Butt, D.P., Joyce, E.L., Sharp, D.H., 1995. Carbon dioxide disposal in carbonate minerals. Energy 20, 1153–1170.

Langmuir, D., Herman, J.S., 1980. The mobility of thorium in natural waters at low temperatures. Geochim. Cosmochim. Acta 44, 1753–1766.

Le Roux, L.J., Glendenin, L.E., 1963. Half-life of $^{232}Th$. Proc. Natl. Meet. Nucl. Energy 83–94.

Lippard, S. J., Shelton, A. W., Gass, I. G., 1986 The Ophiolite of Northern Oman. The Geological Society, Memoir No. 11. Blackwell Scientific Publications, London.

Ludwig, K.R., Titterington, D.M., 1994. Calculation of $^{230}Th/U$ isochrons, ages, and errors. Geochim. Cosmochim. Acta 58, 5031–5042.

Ludwig, K.A., Kelley, D.S., Butterfield, D.A., Nelson, B.K., Früh-Green, G.L., 2006. Formation and evolution of carbonate chimneys at the Lost City hydrothermal field. Geochim. Cosmochim. Acta 70 3625–2645.

Ludwig, K.A., Shen, C.-C., Kelley, D.S., Cheng, H., Edwards, L.R., 2011. U–Th systematics and $^{230}Th$ ages of carbonate chimneys at the Lost City hydrothermal field. Geochim. Cosmochim. Acta 75, 1869–1888.

Luo, Y., Ku, T.-L., 1991. U-series isochron dating: a generalized method employing total sample dissolution. Geochim. Cosmochim. Acta 55, 555–564.

Ma, L., Chabaux, F., Pelt, E., Blaes, E., Jin, L., Brantley, S., 2010. Regolith production rates calculated with uranium-series isotopes at Susquehanna/Shale Hills Critical Zone Observatory. Earth Planet. Sci. Lett. 297, 211–225.

Mathieu, D., Bernat, M., Nahon, D., 1995. Short-lived U and Th isotope distribution in a tropical laterite derived from granite (Pitinga river basin, Amazonia, Brazil): application to assessment of weathering rate. Earth Planet. Sci. 136, 703–714.

Matter, J.M., Kelemen, P.B., 2009. Permanent storage of carbon dioxide in geological reservoirs by mineral carbonation. Nat. Geosci. 2, 837–841.

Mervine, E.M., Humphris, S.E., Sims, K.W.W., Kelemen, P.K., Jenkins, W.J., 2014. Carbonation rates of peridotite in the Samail Ophiolite, Sultanate of Oman, constrained through $^{14}C$ dating and stable isotopes. Geochim. Cosmochim. Acta 126, 371–397.

Mitchell, R.H., 1986. Kimberlites: Mineralogy, Geochemistry, and Petrology. Plenum Press, New York.

Neal, C., Stanger, G., 1983. Hydrogen generation from mantle source rocks in Oman. Earth Planet. Sci. Lett. 66, 315–320.

Neal, C., Stanger, G., 1984. Calcium and magnesium-hydroxide precipitation from alkaline groundwaters in Oman, and their significance to the process of serpentinization. Mineral. Mag. 48, 237–241.

Neal, C., Stanger, G., 1985. Past and present serpentinization of ultramafic rocks: an example from the Semail ophiolite nappe of northern Oman. In: Drewer, J.I. (Ed.), The Chemistry of Weathering. D. Reidel Publishing Company, Holland, pp. 249–275.

Nicolas, A., Boudier, F., Ildefonse, V., Ball, E., 2000. Accretion of Oman and United Arab Emirates ophiolite—discussion of a new structural map. Mar. Geophys. Res. 21, 147–149.

Osmond, J.K., May, J.P., Tanner, W.F., 1970. Age of the Cape Kennedy barrier-and-lagoon complex. J. Geophys. Res. 75, 469–479.

Paukert, A.N., Matter, J.M., Kelemen, P.B., Shock, E.L., Havig, J.R., 2012. Reaction path modeling of enhanced *in situ* $CO_2$ mineralization for carbon sequestration in the peridotite of the Samail Ophiolite, Sultanate of Oman. Chem. Geol. 330–331, 86–100.

Pelt, E., Chabaux, F., Innocent, C., Navarre-Sitchler, A.K., Sak, P.B., Brantley, S.L., 2008. Uranium–thorium chronometry of weathering rinds: rock alteration rate 104 and paleoisotopic record of weathering fluids. Earth Planet. Sci. 105 (Letters 276), 98–105 (103).

Porcelli, D., Swarzneski, P.W., 2003. The behavior of U- and Th-series nuclides in groundwater. In: Bourdon, B., Henderson, G.M., Lundstrom, C.C., Turner, S.P. (Eds.), Uranium-Series Geochemistry. Reviews in Mineralogy and Geochemistry 52, pp. 363–406.

Power, I.M., Wilson, S.A., Thom, J.M., Dipple, G.M., Gabites, J.E., Southam, G., 2009. The hydromagnesite playas of Atlin, British Columbia, Canada: a biogeochemical model for $CO_2$ sequestration. Chem. Geol. 260, 286–300.

Pronost, J., Beaudoin, G., Tremblay, J., Larachi, F., Duchesne, J., Hébert, R., Constantin, M., 2011. Carbon sequestration kinetic and storage capacity of ultramafic mining waste. Environ. Sci. Technol. 45, 9413–9420.

Przybylowicz, W., Schwarcz, H.P., Latham, A.G., 1991. Dirty calcites 2. Uranium series dating of artificial calcite-detritus mixtures. Chem. Geol. 86, 161–178.

Rasbury, E.T., Cole, J.M., 2009. Directly dating geologic events: U–Pb dating of carbonates. Rev. Geophys. 47, 1–27.

Richter, S., Goldberg, S.A., 2003. Improved techniques for high accuracy isotope ratio measurements of nuclear materials using thermal ionization mass spectrometry. Int. J. Mass Spectrom. 229, 181–197.

Rosholt, J.N., Doe, B.R., Tatsumoto, M., 1966. Evolution of the isotopic composition of uranium and thorium in soil profiles. Geol. Soc. Am. Bull. 77, 987–1004.

Rosholt, J.N., Bush, C.A., Shroba, R.R., Pierce, K.L., Richmond, G.M., 1985. Uranium-trend dating and calibrations for Quaternary sediments. Open-File Report 85–299. U.S. Geological Survey, Lakewood, Colorado, p. 48.

Scholz, D., Hoffmann, D., 2008. $^{230}Th/U$-dating of fossil corals and speleothems. Quat. Sci. J. 57, 52–76.

Schwarcz, H.P., Latham, A.G., 1989. Dirty calcites 1. Uranium-series dating of contaminated calcite using leachates alone. Chem. Geol. 80, 35–42.

Searle, M.P., Cox, J., 1999. Tectonic setting, origin, and obduction of the Oman ophiolite. Geol. Soc. Am. Bull. 111, 104–122.

Searle, M.P., Cox, J., 2002. Subduction zone metamorphism during formation and emplacement of the Semail ophiolite in the Oman Mountains. Geol. Mag. 139, 241–255.

Seifritz, W., 1990. $CO_2$ disposal by means of silicates. Nature 345, 486.

Sims, K.W.W., Hart, S.R., Reagen, M.K., Blusztajn, J., Staudigel, H., Sohn, R.A., Layne, G.D., Ball, L.A., Andrews, J., 2008a. $^{238}U$–$^{230}Th$–$^{226}Ra$–$^{210}Pb$–$^{210}Po$, $^{232}Th$–$^{228}Ra$, and $^{235}U$–$^{231}$ Pa constraints on the ages and petrogenesis of Vailulu'u and Malumalu Lavas, Samoa. Geochem. Geophys. Geosyst. 9, 1–30.

Sims, K.W.W., Gill, J.B., Dosseto, A., Hoffman, D.L., Lundstrom, C.C., Williams, R.W., Ball, L., Tollstrup, D., Turner, S., Prytulak, J., Glessner, J.J.G., Standish, J.J., Elliot, T., 2008b. An inter-laboratory assessment of the thorium isotopic composition of synthetic and rock reference materials. Geostand. Geoanal. Res. 32, 65–91.

Streit, E., Kelemen, P., Eiler, J., 2012. Coexisting serpentine and quartz from carbonate-bearing serpentinized peridotite in the Samail Ophiolite, Oman. Contrib. Mineral. Petrol. 164, 821–837.

Surour, A.A., Arafa, E.H., 1997. Ophicarbonates: calichified serpentinites from Gebel Mohagara, Wadi Ghadir area, Eastern Desert, Egypt. J. Afr. Earth Sci. 24, 315–324.

Szabo, B.J., Rosholt, J.N., 1982. Surficial continental sediments. In: Ivanovich, M., Harmon, R.S. (Eds.), Uranium Series Disequilibrium: Applications to Environmental Problems. Claredon Press, London, pp. 257–260.

Thompson, W.G., Spiegelman, M.W., Goldstein, S.L., Speed, R.C., 2003. An open system model for U-series age determinations of fossil corals. Earth Planet. Sci. Lett. 210, 365–381.

Trommsdorff, V., Evans, B.W., 1977. Antigorite-ophicarbonates: contact metamorphism in Valmalenco, Italy. Contrib. Mineral. Petrol. 62, 301–312.

Trommsdorff, V., Evans, B.W., Pfeifer, H.R., 1980. Ophicarbonate rocks: metamorphic reactions and a possible origin. Arch. Sci. Genève 33, 361–364.

Villemant, B., Feuillet, N., 2003. Dating open systems by the $^{238}U$–$^{234}U$–$^{230}Th$ method: application to Quaternary reef terraces. Earth Planet. Sci. Lett. 210, 105–118.
Wilson, S.A., Raudseep, M., Dipple, G.M., 2006. Verifying and quantifying carbon fixation in minerals from serpentine-rich mine tailings using the Rietveld method with X-ray powder diffraction data. Am. Mineral. 91, 1331–1341.
Wilson, S.A., Raudsepp, M., Dipple, G.M., 2009a. Quantifying carbon fixation in trace minerals from processed kimberlite: a comparative study of quantitative methods using X-ray powder diffraction data with applications to the Diavik Diamond Mine, Northwest Territories, Canada. Appl. Geochem. 24, 95–112.
Wilson, S.A., Dipple, G.M., Power, I.M., Thom, J.M., Anderson, R.G., Raudsepp, M., Gabites, J.E., Southam, G., 2009b. Carbon dioxide fixation within mine wastes of ultramafic hosted ore deposits: examples from the Clinton Creek and Cassiar chrysotile deposits, Canada. Econ. Geol. 104, 95–112.
Woodhead, J., Pickering, R., 2012. Beyond 500 ka: progress and prospects in the U–Pb chronology of speleothems, and their application to studies in paleoclimate, human evolution, biodiversity, and tectonics. Chem. Geol. 322–323, 290–299.